

NUMERICAL SOLUTION OF THE NAVIER-STOKES EQUATIONS FOR ARBITRARY TWO-DIMENSIONAL AIRFOILS*

By Frank C. Thames, Joe F. Thompson, and C. Wayne Mastin
Mississippi State University

SUMMARY

A method of numerical solution of the Navier-Stokes equations for the flow about arbitrary airfoils or other bodies is presented. This method utilizes a numerically generated curvilinear coordinate system having a coordinate line coincident with the body contour. Streamlines, velocity profiles, and pressure and force coefficients for several airfoils and an arbitrary rock are given. Potential flow solutions are also presented. The procedure is also capable of treating multiple-element airfoils, and potential flow results are presented therefor.

INTRODUCTION

It is imperative in numerical solution of the Navier-Stokes equations that the boundary conditions be represented accurately in the finite-difference formulation, for the region in the immediate vicinity of solid surfaces is generally dominant in determining the character of the flow. The pressure and forces on solid bodies are directly dependent on the large gradients that prevail in this region near the surface, and accurate pressure and force coefficients require that these large gradients be represented accurately. This problem is accentuated at higher Reynolds numbers as the gradients become more severe.

Therefore, almost all numerical solutions of the Navier-Stokes equations generated to date have treated bodies for which a natural coordinate system is available - circles, ellipses, spheres, Joukowski airfoils, and so forth. (Natural coordinate systems as defined here are those for which the body contour under consideration coincides with a constant coordinate line.) The paper by Mehta and Lavan (ref. 1) has given a solution about a modified Joukowski airfoil accomplished by generating a natural coordinate system with a conformal Joukowski transformation and solving the Navier-Stokes equations on this system. The basic Joukowski transformation was modified somewhat by rounding the trailing edge and contracting the coordinates near the body. Only one case

*Research sponsored by NASA Langley Research Center under Grant
NGR 25-001-055.

was run – a stalled flow at a 15° angle of attack and a Reynolds number of 1000. The method is limited to those bodies which can be generated by the Joukowski transformation (symmetric and cambered Joukowski airfoils, flat plates, and circular and elliptic cylinders) and does not have general applicability. Arbitrary two-dimensional bodies have not been successfully attacked as yet, primarily because of the difficulty of accurate representation of the boundary conditions and the large gradients near solid surfaces when no coordinate line is coincident with the body contour. Some solutions have been attempted with interpolation between grid points for boundaries not coincident with coordinate lines, but this necessarily introduces irregularity into an otherwise smooth boundary and places the most inaccurate difference representation in precisely the region of greatest sensitivity. Dawson (ref. 2) attempted to create a method for general bodies by the use of two uniform rectangular grids: a fine inner grid surrounding the body and extending for perhaps one characteristic body dimension, and a coarse outer grid surrounding the inner grid and extending outward for perhaps 10 to 12 body diameters. The two grids overlap to allow for accurate transition between the two mesh systems. Only a circular cylinder solution was attempted, and this solution was restricted to small Reynolds numbers ($R \leq 1000$) because of boundary instabilities.

A method of automatic numerical generation of a general curvilinear coordinate system with coordinate lines coincident with all boundaries of a general multiconnected region containing any number of arbitrarily shaped bodies has, however, been developed which should alleviate this problem with arbitrary bodies (ref. 3). The curvilinear coordinates are generated as the solution of two elliptic partial differential equations with Dirichlet boundary conditions, one coordinate being specified to be constant on each of the boundaries, and a distribution of the other being specified along the boundaries. These equations are solved in finite-difference approximation by successive over-relaxation (SOR) iteration. No restrictions are placed on the shape of the boundaries, which may even be time dependent, and the method is not restricted to two dimensions or single bodies. Coordinate lines may be concentrated as desired along the boundaries. Spacing of the coordinate lines encircling the body may be controlled by adjusting parameters in the partial differential equations for the coordinates.

Regardless of the shape and number of the bodies and regardless of the spacing of the curvilinear coordinate lines, all numerical computations, both to generate the coordinate system and subsequently to solve the Navier-Stokes equations on the coordinate system, are done on a rectangular grid with a square mesh, that is, in the transformed plane. It is also possible to cause the natural coordinate system to change in time as desired and still have all computation done on the fixed rectangular grid with square mesh. This allows the curvilinear coordinate system in the physical plane to deform with a deforming body, blast front, shock, free surface, or any other boundary, keeping a coordinate line always coincident with the boundary at all times. The physical coordinate

system has been, in effect, eliminated from the problem, at the expense of adding two elliptic equations to the original system.

Since the curvilinear coordinate system has coordinate lines coincident with the surface contours of all bodies present, all boundary conditions may be expressed at grid points. Also, normal derivatives on the bodies may be represented by using only finite differences between grid points on coordinate lines, without need of any interpolation, even though the coordinate system is not orthogonal at the boundary. Numerical solutions for the lifting and nonlifting potential flow about Kármán-Trefftz airfoils obtained with this coordinate-system generation show excellent comparison with the analytic solutions.

This method of automatic body-fitted curvilinear coordinate generation has been used to construct a finite-difference solution of the full, incompressible, time-dependent, Navier-Stokes equations for the laminar viscous flow about arbitrary two-dimensional airfoils or any other two-dimensional body (ref. 4). The Navier-Stokes equations are written in the vorticity-stream-function formulation, with the vorticity on the body being determined by a type of false-position iteration so that the no-slip boundary condition is satisfied. The solution is implicit in time, the vorticity and the stream-function equations being solved simultaneously at each time step by SOR iteration. A method of controlling the spacing of the coordinate lines encircling the body has been developed in order to treat high Reynolds number flow, since the coordinate lines must concentrate near the surface to a greater degree as the Reynolds number increases. The solution is designed to provide the velocity field, the surface-pressure distribution, and the lift, drag, and moment coefficients. Results are given for separated flow over two airfoils and an arbitrary rock. Initial application to multiple airfoils has also been made.

SYMBOLS

a, b, c, d	coefficients in equations (5)
C_A	axial-force coefficient
C_D	drag coefficient
C_{DF}	friction-drag coefficient
C_{DP}	pressure-drag coefficient
C_L	lift coefficient

C_N	normal-force coefficient
C_p	pressure coefficient
C_p^*	pressure coefficient referenced to trailing-edge pressure
D	differential operator; two-dimensional region (fig. 1)
D^*	rectangular region (fig. 1)
ds	increment of arc length along body surface
E	maximum norm
\underline{F}	force on body
f	function
i, j	computational grid points; $i = 1 \dots I$; $j = 1 \dots J$
$\underline{i}, \underline{j}$	unit vectors
J	Jacobian
k	iteration counter
M, N	summation limits (eqs. (5))
m, n	indices
\underline{n}	unit vector normal to body surface
P, Q	amplitude factors (eqs. (5))
p	pressure
R	Reynolds number
S	body surface

T_n	stress vector on body surface
t	time
t_n	current time
V	velocity
V_t	tangential velocity component
x, y	physical coordinates (nondimensionalized by airfoil chord)
α, β, γ	coefficients of natural coordinate transformation (eqs. (3))
$\Gamma_1, \Gamma_2, \dots, \Gamma_8$	curves in physical plane
$\Gamma_1^*, \Gamma_2^*, \dots, \Gamma_8^*$	curves in transformed plane
ϵ	convergence factor
δ	relaxation factor
θ	free-stream angle of attack
λ	coefficient in stream-function equation
ξ, η	transformed coordinates
σ, τ	coefficients in equation (9a)
ψ	stream function
ψ_b	value of ψ at body
ω	vorticity
ω_b	value of ω at body

Superscripts:

L lower surface

U upper surface

* transformation

Subscripts:

L lower surface

o trailing edge (fig. 4)

T.E. trailing edge

U upper surface

x,y differentiation with respect to x or y

ξ, η differentiation with respect to ξ or η

∞ free stream

BODY-FITTED CURVILINEAR COORDINATE SYSTEM

Mathematical Development

Let it be desired to transform the two-dimensional, doubly connected region D bounded by two closed contours of arbitrary shape into a rectangular region D^* , as shown in figure 1. The general transformation from the physical plane $[x,y]$ to the transformed plane $[\xi,\eta]$ is given by $\xi = \xi(x,y)$, $\eta = \eta(x,y)$. Similarly, the inverse transformation is given by $x = x(\xi,\eta)$, $y = y(\xi,\eta)$. Derivatives are transformed as follows:

$$f_x = \frac{\partial(f,y)/\partial(\xi,\eta)}{\partial(x,y)/\partial(\xi,\eta)} = \frac{y_\eta f_\xi - y_\xi f_\eta}{J} \quad (1a)$$

$$f_y = \frac{\partial(x,f)/\partial(\xi,\eta)}{\partial(x,y)/\partial(\xi,\eta)} = \frac{-x_\eta f_\xi + x_\xi f_\eta}{J} \quad (1b)$$

where J is the Jacobian of the transformation $J = x_\xi y_\eta - x_\eta y_\xi$.

Since the basic idea of the transformation is to generate transformation functions such that all boundaries are coincident with coordinate lines, the natural coordinates $[\xi, \eta]$ are taken as solutions of some suitable elliptic boundary value problem with one of these coordinates constant on the boundaries. Using Laplace's equation as the generating elliptic system gives

$$\xi_{xx} + \xi_{yy} = 0 \quad (2a)$$

$$\eta_{xx} + \eta_{yy} = 0 \quad (2b)$$

with Dirichlet boundary conditions: $\eta = \text{Constant} = \eta_1$ on Γ_1 , $\eta = \text{Constant} = \eta_2$ on Γ_2 , and $\xi(x, y)$ a multiple-valued solution with a branch of $\xi(x, y)$ specified (but not constant) on Γ_1 and Γ_2 . The curve Γ_1 on the physical plane transforms to the lower boundary Γ_1^* of the transformed plane. Similarly, Γ_2 transforms to Γ_2^* , and so forth. The right and left boundaries of the rectangular transformed plane Γ_3^* and Γ_4^* are coincident in the physical plane. The curve which transforms to these boundaries connects Γ_1 and Γ_2 and determines a branch cut for the multiple-valued function $\xi(x, y)$. Thus the functions and all derivatives are continuous across this cut.

Now since it is desirable to do all numerical computation in the rectangular transformed plane, it is necessary to interchange the dependent and independent variables in equations (2). Thus

$$\alpha x \xi \xi - 2\beta x \xi \eta + \gamma x \eta \eta = 0 \quad (3a)$$

$$\alpha y \xi \xi - 2\beta y \xi \eta + \gamma y \eta \eta = 0 \quad (3b)$$

where

$$\alpha = x_\eta^2 + y_\eta^2 \quad (3c)$$

$$\beta = x_\xi x_\eta + y_\xi y_\eta \quad (3d)$$

$$\gamma = x_\xi^2 + y_\xi^2 \quad (3e)$$

with the transformed boundary conditions: $x = f_1(\xi, \eta_1)$ on Γ_1^* , $y = g_1(\xi, \eta_1)$ on Γ_1^* , $x = f_2(\xi, \eta_2)$ on Γ_2^* , and $y = g_2(\xi, \eta_2)$ on Γ_2^* . (In the present application, x and y are nondimensionalized with respect to the airfoil chord.)

The natural coordinate system so generated has a constant η -line coincident with each boundary in the physical plane. The ξ -lines may be spaced in any manner desired around the boundaries by specification of $[x, y]$ at the equispaced ξ -points on the η_1 - and

η_2 -lines of the transformed plane. Control of the spacing of the η -lines may be exercised by varying the elliptic system of which ξ and η are solutions.

Extension to Multiple Bodies

The same procedure for natural coordinate generation may be extended to regions that are more than doubly connected, that is, have more than two closed boundaries or, equivalently, more than one body or hole within a single outer boundary. The transformation to the rectangular field is illustrated in figure 2.

The method requires that the η -coordinate be equal to the same constant on all the interior boundaries, that is, on all bodies in the field. Let all the bodies be connected by arbitrary cuts and, similarly, one body be connected to the outer boundary by an arbitrary cut. Since the η -coordinate is equal to the same constant on all the bodies, it is, of course, equal to that constant on the cuts between the bodies also. By contrast, the ξ -coordinate is taken constant on the cut between the body and the outer boundary. Since the locations of these cuts in the physical plane are not specified, the specification of η or ξ as constant on a cut does not overspecify the elliptic problem.

Note that all bodies except one are split into two segments. Each cut appears twice on the transformed field boundary, the two segments, of course, corresponding to the two "sides" of the cut in the physical plane and thus being reentrant boundaries with the functions and all derivatives continuous thereon. Thus x and y have been specified on the portions of the lower boundary of the transformed field that correspond to the bodies - Γ_7^* and Γ_8^* for the right body and Γ_1^* for the left body - and also on the entire upper boundary, corresponding to the outer boundary in the physical field. The remaining portions of the lower boundary and the entire side boundaries are reentrant boundaries and, thus, neither require nor allow specification of $[x, y]$ thereon.

Again an elliptic Dirichlet problem is solved to generate the natural coordinates $[x, y]$, as in the previously considered case with only a single body. All computations, both to generate the coordinates and subsequently to solve the partial differential system of interest, are again done on the rectangular field with square mesh in the transformed plane.

Numerical Solution

The relation between the transformed and physical fields for a single airfoil is shown in figure 3(a). The physical coordinates of I points describing the body surface $[x, y]$ provide the boundary conditions along the $j = 1$ line; those of I points on the physical remote boundary, usually a circle with radius 10 or more chords, supply the boundary conditions along the $j = J$ line of the transformed field. Since the side boundaries of the transformed field are reentrant, corresponding to the cut in the physical

plane, then $f_{1,j} = f_{1,j}$ and $f_{I+1,j} = f_{2,j}$ for all j . Note that the values of x and y are not specified on these side boundaries. All derivatives in equations (3) are approximated by second-order, central-difference expressions ($\Delta\xi$ and $\Delta\eta$ are both unity by construction, the actual values of ξ and η being immaterial):

$$(f_\xi)_{ij} \approx \frac{1}{2}(f_{i+1,j} - f_{i-1,j}) \quad (4a)$$

$$(f_\eta)_{ij} \approx \frac{1}{2}(f_{i,j+1} - f_{i,j-1}) \quad (4b)$$

$$(f_{\xi\xi})_{ij} \approx f_{i+1,j} - 2f_{ij} + f_{i-1,j} \quad (4c)$$

$$(f_{\eta\eta})_{ij} \approx f_{i,j+1} - 2f_{ij} + f_{i,j-1} \quad (4d)$$

$$(f_{\xi\eta})_{ij} \approx \frac{1}{4}(f_{i+1,j+1} - f_{i+1,j-1} - f_{i-1,j+1} + f_{i-1,j-1}) \quad (4e)$$

The resulting set of $2I(J - 1)$ nonlinear difference equations, two for each point $[i,j]$ for $i = 1, 2, \dots, I - 1$ and $j = 2, 3, \dots, J - 1$, were solved by accelerated Gauss-Seidel (SOR) iteration. The iteration was considered to have converged when the maximum absolute change on the field between iterations was less than 10^{-5} . A range of acceleration parameters was examined, and a value of 1.85 was nearly optimum for the bodies considered.

The relation between the transformed and physical fields for two airfoils is shown in figure 3(b). The physical coordinates of body 2 at points $i = 1 \dots I_1$, those of body 1 at points $i = I_2 \dots I_3$, and finally the remaining points $i = I_4 \dots I$ on body 2 are input as boundary conditions on the $j = 1$ line in the transformed plane. The remaining points $i = (I_1 + 1) \dots (I_2 - 1)$ and $i = (I_3 + 1) \dots (I_4 - 1)$ on the $j = 1$ line are reentrant points corresponding to the cut between the bodies in the physical plane. Therefore values at these points are not specified, but rather the relations $f_{I_1+k,1} = f_{I_4-k,1}$ and $f_{I_1+k,0} = f_{I_4-k,2}$ for $k = 1 \dots (I_2 - I_1 - 1)$ hold. The rest of the procedure is unchanged from the case of a single airfoil, except that two difference equations at each of the points $[i,1]$ for $i = (I_1 + 1) \dots (I_2 - 1)$ are added to the system, so that the total number of equations is now $2I(J - 1) + 2(I_2 - I_1 - 1)$.

Control of Coordinate System

Several procedures for controlling the spacing of the coordinate lines in the field are available and the general philosophy of such control is discussed in reference 3. One particularly effective procedure is to add exponential inhomogeneous terms to the

Laplace equations for the curvilinear coordinates, so that the coordinates are generated as the solutions of

$$\xi_{xx} + \xi_{yy} = \sum_{m=1}^M a_m \frac{\xi - \xi_m}{|\xi - \xi_m|} \exp(-c_m |\xi - \xi_m|) + \sum_{n=1}^N b_n \frac{\xi - \xi_n}{|\xi - \xi_n|} \exp\left[-d_n \sqrt{(\xi - \xi_n)^2 + (\eta - \eta_n)^2}\right] \equiv P \quad (5a)$$

$$\eta_{xx} + \eta_{yy} = \sum_{m=1}^M a_m \frac{\eta - \eta_m}{|\eta - \eta_m|} \exp(-c_m |\eta - \eta_m|) + \sum_{n=1}^N b_n \frac{\eta - \eta_n}{|\eta - \eta_n|} \exp\left[-d_n \sqrt{(\xi - \xi_n)^2 + (\eta - \eta_n)^2}\right] \equiv Q \quad (5b)$$

where the amplitudes and decay factors are not necessarily the same in the two equations. Here the first terms have the effect of attracting ξ -lines to the ξ_m -lines in the ξ -equation, and attracting η -lines to the η_m -lines in the η -equation. The second terms cause ξ -lines to be attracted to the points $[\xi_n, \eta_n]$ in the ξ -equation, with a similar effect on η -lines in the η -equation.

In the transformed plane these equations become

$$\alpha x_{\xi\xi} - 2\beta x_{\xi\eta} + \gamma x_{\eta\eta} = -J^2(Px_{\xi} + Qx_{\eta}) \quad (6a)$$

$$\alpha y_{\xi\xi} - 2\beta y_{\xi\eta} + \gamma y_{\eta\eta} = -J^2(Py_{\xi} + Qy_{\eta}) \quad (6b)$$

POTENTIAL-FLOW SOLUTION

Laplace Equation and Boundary Conditions

The two-dimensional irrotational flow about any number of bodies may be described by the Laplace equation for the stream function, ψ :

$$\psi_{xx} + \psi_{yy} = 0 \quad (7)$$

with boundary conditions:

On the body surface,

$$\psi(x, y) = \psi_0 \quad (8a)$$

At infinity,

$$\psi(x,y) = y \cos \theta - x \sin \theta \quad (8b)$$

where θ is the angle of attack of the free stream relative to the positive x -axis. Here the stream function is nondimensionalized relative to the airfoil chord and the free-stream velocity. When transformed to the curvilinear coordinate system, this equation becomes

$$\alpha \psi_{\xi\xi} - 2\beta \psi_{\xi\eta} + \gamma \psi_{\eta\eta} + \sigma \psi_{\eta} + \tau \psi_{\xi} = 0 \quad (9a)$$

where α , β , and γ are defined by equations (3c) to (3e) and σ and τ are given by

$$\sigma \equiv \frac{y_{\xi}(Dx) - x_{\xi}(Dy)}{J} \quad (9b)$$

$$\tau \equiv \frac{x_{\eta}(Dy) - y_{\eta}(Dx)}{J} \quad (9c)$$

with

$$Dx \equiv \alpha x_{\xi\xi} - 2\beta x_{\xi\eta} + \gamma x_{\eta\eta} \quad (9d)$$

$$Dy \equiv \alpha y_{\xi\xi} - 2\beta y_{\xi\eta} + \gamma y_{\eta\eta} \quad (9e)$$

Note that Dx and Dy , and hence σ and τ , vanish when no coordinate contraction is used, that is, when the generating system is simply equations (3). The transformed boundary conditions are

On $\eta = \eta_1$ (i.e., on Γ_1^*),

$$\psi(\xi, \eta_1) = \psi_b \quad (10a)$$

On $\eta = \eta_2$ (i.e., on Γ_2^*),

$$\psi(\xi, \eta_2) = y(\xi, \eta_2) \cos \theta - x(\xi, \eta_2) \sin \theta \quad (10b)$$

The uniqueness is implied by insisting that the solution be periodic in $-\infty < \xi < \infty$, $\eta_1 \leq \eta \leq \eta_2$. The coefficients α , β , γ , σ , and τ are calculated during the generation of the natural coordinate system. For the approximation of equations (9), second-order, central differences are used for all derivatives, and the resulting difference equation is solved by accelerated Gauss-Seidel (SOR) iteration on the rectangular transformed field.

The solution of equations (9) on the transformed field is constructed in the same manner that has been previously described for the solution of equations (3). The single equation (9a) replaces the two equations (3a) and (3b), and the boundary conditions are

given by equations (10). The total number of difference equations thus is $I(J - 1)$ for a single airfoil and $I(J - 1) + (I_2 - I_1 - 1)$ for two airfoils.

Kutta Condition

The boundary value of ψ on the body, ψ_b is determined by imposing the Kutta condition. The Kutta condition arises from physical considerations and basically asserts that the flow must leave the sharp trailing edge of an airfoil section in a smooth fashion. In a mathematical sense this smoothness condition is guaranteed by insisting that the velocity on the surface of the airfoil be continuous. The continuity implies that the limit of the velocity at any point on the surface exists and is the same regardless of the path along which this point is approached. In particular, the velocity at the trailing edge of the airfoil must be the same when approached from the upstream direction along the upper and lower surfaces. It is easily shown that the above ideas imply that the trailing edge is a stagnation point for airfoils having an included trailing-edge angle greater than zero, but only a common (possibly nonzero) upper and lower surface velocity limit is required for cusped trailing edges. The common-limit condition has also been applied by Giesing (ref. 5) in a solution utilizing superposition of singularities.

Since the normal velocity component vanishes identically on the airfoil surface, only the tangential velocity component need be considered. If $V_t(\eta)$ is the component of \vec{V} tangent to a constant η -line, then

$$V_t(\eta_1) = \frac{\sqrt{\gamma}\psi_\eta}{J} \quad (11)$$

On the surface the ξ -derivatives are approximated by the second-order, central-difference expressions of equation (4a), as in the interior of the field, at all points except those on the cut $i = 1$ and $i = I$, where second-order, one-sided expressions are used. Thus

$$(f_\xi)_{1,1} = \frac{1}{2}(-f_{3,1} + 4f_{2,1} - 3f_{1,1}) \quad (12a)$$

$$(f_\xi)_{I,1} = \frac{1}{2}(f_{I-2,1} - 4f_{I-1,1} + 3f_{I,1}) \quad (12b)$$

The η -derivatives on the surface are approximated at all points by similar one-sided expressions:

$$(f_\eta)_{i,1} = \frac{1}{2}(-f_{i,3} + 4f_{i,2} - 3f_{i,1}) \quad (12c)$$

To implement the condition of a common velocity limit numerically, the tangential velocity component at the airfoil trailing edge is approximated by a three-point, quadratic

extrapolation in which the three points on the airfoil surface immediately adjacent to the trailing-edge point on both upper and lower surfaces are utilized. This procedure is illustrated in figure 4. The extrapolated values are

$$(\underline{v}_t)_o^{(U)} = 3(\underline{v}_t)_{1U,1} - 3(\underline{v}_t)_{2U,1} + (\underline{v}_t)_{3U,1} \quad (13a)$$

$$(\underline{v}_t)_o^{(L)} = 3(\underline{v}_t)_{1L,1} - 3(\underline{v}_t)_{2L,1} + (\underline{v}_t)_{3L,1} \quad (13b)$$

where the subscripts o , $1U$, $2U$, $3U$, $1L$, $2L$, and $3L$ refer to the ξ -field position as indicated in figure 4. All η -field position indices are of course unity. The common-limit condition is then

$$(\underline{v}_t)_o^{(U)} = (\underline{v}_t)_o^{(L)} \quad (14)$$

Superposition of Solutions

Since the system to be solved is linear in ψ , the solution for a single airfoil at any angle of attack may be obtained by superposing three component solutions: (1) a solution at 0° angle of attack with no circulation, (2) a solution at 90° angle of attack with no circulation, and (3) a solution with circulation but zero free-stream velocity. These three component solutions, written $\psi^{(k)}(\xi, \eta)$, where $k = 1, 2, 3$, each satisfy equations (9), with the respective boundary conditions

$$\psi_{i,1}^{(1)} = 0 \quad (i = 1 \dots I) \quad (15a)$$

$$\psi_{i,J}^{(1)} = y_{i,J} \quad (i = 1 \dots I) \quad (15b)$$

$$\psi_{i,1}^{(2)} = 0 \quad (i = 1 \dots I) \quad (16a)$$

$$\psi_{i,J}^{(2)} = -x_{i,J} \quad (i = 1 \dots I) \quad (16b)$$

$$\psi_{i,1}^{(3)} = 1 \quad (i = 1 \dots I) \quad (17a)$$

$$\psi_{i,J}^{(3)} = 0 \quad (i = 1 \dots I) \quad (17b)$$

The complete solution with arbitrary circulation then is

$$\psi(\xi, \eta; \lambda) = \psi^{(1)}(\xi, \eta) \cos \theta + \psi^{(2)}(\xi, \eta) \sin \theta + \lambda \psi^{(3)}(\xi, \eta) \quad (18)$$

The Kutta condition is then satisfied by choosing the coefficient λ such that equation (14) is satisfied. Thus it is only necessary to solve the system of difference equations three times for a given airfoil. The solution at any angle of attack may then be obtained without re-solving the difference system.

Surface Pressure and Force Coefficients

The pressure coefficient at any point in the field may be obtained from the velocities via the Bernoulli equation, which in the present nondimensional variables is

$$C_p = 1 - |\tilde{V}|^2 \quad (19)$$

On the body surface this becomes, through use of equation (11),

$$C_p = 1 - \frac{\gamma}{J^2} \psi_\eta^2 \quad (20)$$

with the derivative evaluated by a second-order, one-sided difference expression. The nondimensional force on the body is given by

$$\mathbf{F} = -\oint C_p \mathbf{n} \, ds \quad (21)$$

where \mathbf{n} is the unit outward normal to the surface, and ds is an increment of arc length along the surface. The lift and drag coefficients are

$$C_L = \oint C_p (-x_\xi \cos \theta - y_\xi \sin \theta) \, d\xi \quad (22a)$$

$$C_D = \oint C_p (y_\xi \cos \theta + x_\xi \sin \theta) \, d\xi \quad (22b)$$

These integrals were evaluated with numerical quadrature by means of the trapezoidal rule.

Multiple Airfoils

With two airfoils, the boundary condition of equation (8a) is replaced by the two boundary conditions:

On the surface of body 1,

$$\psi(x, y) = \psi_1 \quad (23a)$$

On the surface of body 2,

$$\psi(x,y) = \psi_2 \quad (23b)$$

With reference to figure 3 and the discussion in the previous section of the coordinate system solution, these boundary conditions become, in the transformed field,

$$\psi_{i,1} = \psi_1 \quad (i = I2 \dots I3) \quad (24a)$$

$$\psi_{i,1} = \psi_2 \quad (i = 1 \dots I1 \text{ and } i = I4 \dots I) \quad (24b)$$

As in the case of the coordinate system solution, the remaining portions of the $j = 1$ line are reentrant boundaries, so that points thereon are treated as field points rather than boundary points. The ξ -derivatives at the surface points I1, I2, I3, and I4 on the cuts between the bodies are also evaluated by using the one-sided expressions of equations (12) in the calculation of the velocity on the surface.

The Kutta condition must be applied on each body. Therefore, a fourth component solution is added, and the four component solutions each satisfy equation (9a), with the boundary conditions

$$\psi_{i,1}^{(1)} = 0 \quad (i = 1 \dots I1, I2 \dots I3, I4 \dots I) \quad (25a)$$

$$\psi_{i,J}^{(1)} = y_{i,J} \quad (i = 1 \dots I) \quad (25b)$$

$$\psi_{i,1}^{(2)} = 0 \quad (i = 1 \dots I1, I2 \dots I3, I4 \dots I) \quad (26a)$$

$$\psi_{i,J}^{(2)} = -x_{i,J} \quad (i = 1 \dots I) \quad (26b)$$

$$\psi_{i,1}^{(3)} = 0 \quad (i = 1 \dots I1, I4 \dots I) \quad (27a)$$

$$\psi_{i,1}^{(3)} = 1 \quad (i = I2 \dots I3) \quad (27b)$$

$$\psi_{i,J}^{(3)} = 0 \quad (i = 1 \dots I) \quad (27c)$$

$$\psi_{i,1}^{(4)} = 1 \quad (i = 1 \dots I1, I4 \dots I) \quad (28a)$$

$$\psi_{i,1}^{(4)} = 0 \quad (i = I2 \dots I3) \quad (28b)$$

$$\psi_{i,J}^{(4)} = 0 \quad (i = 1 \dots I) \quad (28c)$$

The complete solution with arbitrary circulation about each body is

$$\psi(\xi, \eta; \lambda_1, \lambda_2) = \psi^{(1)}(\xi, \eta) \cos \theta + \psi^{(2)}(\xi, \eta) \sin \theta + \lambda_1 \psi^{(3)}(\xi, \eta) + \lambda_2 \psi^{(4)}(\xi, \eta) \quad (29)$$

The Kutta condition is then satisfied by choosing the coefficients λ_1 and λ_2 such that equation (14) is satisfied on each body. This requires only the simultaneous solution of two linear algebraic equations. Generalizing to N bodies, it is necessary to solve the difference equation system $N+2$ times for a given multiple airfoil system. The solution at any orientation of the free stream may then be obtained without re-solving the difference system.

Results and Comparisons

The coordinate system for a Kármán-Trefftz airfoil having an integral flap is shown in figure 5, and the streamlines and pressure distribution for this airfoil are compared with the analytic solution (ref. 6) in figure 6. Similar excellent comparisons have been obtained with other Kármán-Trefftz airfoils. Figure 7 shows the coordinate system for a Liebeck laminar airfoil, the solution for which is compared with experimental results (ref. 7) for the pressure distribution and lift curve in figure 8. Finally, the coordinate system for a multiple-element airfoil is shown in figure 9, with the streamlines and pressure distributions shown in figure 10. Here coordinate system control was employed as discussed above to attract the coordinate lines into the concave region formed by the intersections of the cut between the airfoils.

APPLICATION TO THE NAVIER-STOKES EQUATIONS

Basic Equations

The stream-function—vorticity formulation of the two-dimensional, incompressible, viscous-flow equations is given by

$$\omega_t + \psi_y \omega_x - \psi_x \omega_y = \frac{\omega_{xx} + \omega_{yy}}{R} \quad (30)$$

$$\psi_{xx} + \psi_{yy} = -\omega \quad (31)$$

where ψ is the nondimensional stream function, ω the nondimensional vorticity, and R the Reynolds number based on the characteristic velocity and length used to nondimensionalize the basic equations. The transformed equations are

$$\omega_t + \frac{\psi_\eta \omega_\xi - \psi_\xi \omega_\eta}{J} = \frac{\alpha \omega_{\xi\xi} - 2\beta \omega_{\xi\eta} + \gamma \omega_{\eta\eta} + \sigma \omega_\eta + \tau \omega_\xi}{J^2 R} \quad (32)$$

$$\alpha \psi_{\xi\xi} - 2\beta \psi_{\xi\eta} + \gamma \psi_{\eta\eta} + \sigma \psi_\eta + \tau \psi_\xi = -J^2 \omega \quad (33)$$

where the coordinate system parameters α , β , γ , J , σ , and τ have already been given. Recall that these coordinate system parameters are fixed and need be calculated only once.

Boundary Conditions

The boundary conditions are given by

On the body surface,

$$\psi(x, y, t) = \psi_b = \text{Constant} \quad (34a)$$

$$\frac{\partial \psi}{\partial n}(x, y, t) = 0 \quad (34b)$$

At infinity,

$$\psi(x, y, t) = y \cos \theta - x \sin \theta \quad (35a)$$

$$\omega(x, y, t) = 0 \quad (35b)$$

where \underline{n} is the unit vector normal to the body surface. The function describing the variation of the vorticity on the body $\omega_b(x, y, t)$ is unknown and must be calculated as part of the solution. Initial conditions at $t = 0$ are those resulting from an impulsive start. Equations (34) and (35) may be transformed to yield boundary conditions for equations (32) and (33) in the transformed plane. This procedure yields the following relations:

On $\eta = \eta_1$ (i.e., on Γ_1^*),

$$\psi(\xi, \eta_1, t) = \psi_b = \text{Constant} \quad (36a)$$

$$\frac{\sqrt{\gamma}}{J} \psi_\eta(\xi, \eta_1, t) = 0 \quad (36b)$$

On $\eta = \eta_2$ (i.e., on Γ_2^*),

$$\psi(\xi, \eta_2, t) = y(\xi, \eta_2) \cos \theta - x(\xi, \eta_2) \sin \theta \quad (37a)$$

$$\omega(\xi, \eta_2, t) = 0 \quad (37b)$$

where η_1 and η_2 are the values of the η -coordinate for contours Γ_1^* and Γ_2^* , respectively, in the transformed plane (fig. 1). The condition specified by equation (36b) guarantees that the velocity component tangent to the transformed body surface vanishes on the body surface. Since the component normal to the body surface vanishes identically, the satisfaction of equation (36b) implies that the viscous no-slip condition is satisfied on the body surface (i.e., along Γ_1^* , or equivalently Γ_1).

Most solutions in the computational fluids field have relied on a modified evaluation of equation (33) on the boundary to determine the vorticity on the body surface $\omega_b(\xi, \eta_1, t)$. The modification is introduced in an attempt to insure that equation (36b) holds – that is, to satisfy the no-slip condition. A variety of numerical procedures along these lines are documented in reference 8. The principal problem encountered with such an approach is that the vanishing of the tangential velocity component is implied only indirectly rather than directly. Israeli (ref. 9) has shown that these procedures are not only unreliable in producing a zero tangential component, but may, in fact, even be numerically divergent. Israeli suggests that $\omega_b(\xi, \eta_1, t)$ be calculated with an iterative algorithm of the form

$$\omega_b^{(k+1)}(\xi_i, \eta_1, t_n) = \omega_b^{(k)}(\xi_i, \eta_1, t_n) - \delta \left[\frac{\partial \psi}{\partial n}(\xi_i, \eta_1, t_n) \right] \quad (38)$$

for all $1 \leq i \leq I - 1$, where ξ_i refers to the ξ -position along the body, η_1 denotes the η -value for contour Γ_1^* , t_n is the current time, k denotes the iteration counter at step t_n , and δ is a relaxation factor (possibly variable). Obviously, such a procedure can only be employed with implicit methods which require iteration of the parabolic vorticity equation at each time increment. Note that convergence of the vector sequence $\omega_b^{(k)}(\xi_i, \eta_1, t_n)$ implies convergence of $\left[\frac{\partial \psi}{\partial n}(\xi_i, \eta_1, t_n) \right]^{(k)}$ to that function which inherently satisfies the no-slip boundary condition.

Pressure Coefficients

If the primitive variable formulation of the Navier-Stokes equations (velocity-pressure) is evaluated on the body surface, the time derivative and inertia terms vanish to yield

$$\nabla p = \frac{1}{R} \nabla^2 \underline{v} \quad (39)$$

where p is the nondimensional pressure, \underline{v} the nondimensional velocity, and R the Reynolds number based on the characteristic flow parameters. Utilizing a vector identity to eliminate $\nabla^2 \underline{v}$ gives

$$\nabla p = \frac{1}{R}(j\omega_x - i\omega_y) \quad (40)$$

The pressure differential in the transformed plane then is

$$dp = \frac{1}{RJ}(\beta\omega_\xi - \gamma\omega_\eta)d\xi \quad (41)$$

Integration of equation (41) along Γ_1 starting at the trailing-edge position yields

$$C_p^*(\xi) \equiv p(\xi) - p_{T.E.} = \frac{1}{R} \int_{\xi_{T.E.}}^{\xi} \frac{1}{J}(\beta\omega_\xi - \gamma\omega_\eta)d\xi' \quad (42)$$

where $\xi_{T.E.}$ is the ξ -value corresponding to the body trailing edge. The symbol C_p^* is used instead of the more conventional C_p to indicate that the reference pressure is the trailing-edge value $p_{T.E.}$ rather than the free-stream value p_∞ . Note that all quantities in equation (42) must be evaluated on the body surface (i.e., along $\eta = \eta_1$). Central-difference approximations were used for all ξ -derivatives appearing in equation (42), while second-order one-sided expressions were used for the η -derivatives. The numerical quadrature was performed by the trapezoidal rule.

Force Coefficients

The force coefficients associated with the stress vector are obtained by integrating the stress vector over the body surface. Let $\underline{F} = iC_A + jC_N$ be the total force acting on the body and let $\underline{T}_n = i(T_n)_1 + j(T_n)_2$ be the stress vector on the body surface having outward unit normal \underline{n} . Then,

$$\underline{F} = \int_S \underline{T}_n dS \quad (43)$$

where S is the body surface. The stress vector components $(T_n)_1$ and $(T_n)_2$ may be expressed in terms of the primitive variables as

$$(T_n)_1 = -2pn_1 + 4(V_1)_x \frac{n_1}{R} + 2[(V_1)_y + (V_2)_x] \frac{n_2}{R} \quad (44a)$$

$$(T_n)_2 = -2pn_2 + 2[(V_2)_x + (V_1)_y] \frac{n_1}{R} + 4(V_2)_y \frac{n_2}{R} \quad (44b)$$

where n_1 and n_2 are the x- and y-components of the normal to the body surface \underline{n} . The lift and drag coefficients may then be calculated by means of the conventional wind-axis transformation as follows:

$$C_D = 2 \int_{\xi_{\min}}^{\xi_{\max}} (y_{\xi} \cos \theta - x_{\xi} \sin \theta) C_p^* d\xi + 2 \int_{\xi_{\min}}^{\xi_{\max}} \frac{y_{\xi} \sin \theta - x_{\xi} \cos \theta}{R} \omega d\xi \quad (45a)$$

$$C_L = -2 \int_{\xi_{\min}}^{\xi_{\max}} \left[\cos \theta \left(x_{\xi} C_p^* - \frac{y_{\xi} \omega}{R} \right) + \sin \theta \left(y_{\xi} C_p^* - \frac{x_{\xi} \omega}{R} \right) \right] d\xi \quad (45b)$$

The two integrals in equations (45) are referred to as the pressure and friction drag coefficients and are denoted C_{DP} and C_{DF} , respectively. These integrals were evaluated numerically by use of the trapezoidal rule. The ξ -derivatives were approximated with second-order central-difference expressions.

Difference Equations

A first-order backward difference is used to approximate the time derivative, while second-order central differences are used for the space derivatives in equations (32) and (33). The resulting coupled difference equations, two for each point in the field, were solved simultaneously by point SOR iteration at each time step.

Implementation of the Boundary Conditions

As indicated earlier, the basic idea used to calculate the vorticity on the body surface $\omega_b(\xi, \eta, t)$ is to select this function so that the no-slip condition is satisfied. An approach suggested by Israeli (ref. 9) has already been cited in equation (38). This is basically the parallel-chord method (see ref. 10) and has only a linear convergence rate. Another method similar to false-position iteration was used to accelerate the convergence. The iterative sequence is generated by the algorithm

$$\omega_{i,1}^{(k+1)} = \omega_{i,1}^{(k)} - \delta \frac{\omega_{i,1}^{(k)} - \omega_{i,1}^{(k-1)}}{\left(\frac{\sqrt{\gamma}}{J} \psi_{\eta}\right)_{i,1}^{(k)} - \left(\frac{\sqrt{\gamma}}{J} \psi_{\eta}\right)_{i,1}^{(k-1)}} \left(\frac{\sqrt{\gamma}}{J} \psi_{\eta}\right)_{i,1}^{(k)} \quad (46)$$

where δ is again an acceleration parameter. The derivatives in this equation were approximated with second-order one-sided differences for the η -derivatives and central differences for the ξ -derivatives. Another method was used when numerical overflow problems were encountered with the quotient in equation (46). This consisted of modifying the second term on the right side of equation (38) with the algebraic sign of the difference quotient. Several other approaches documented in Roache (ref. 8) were also tried. None of these were as successful as the methods discussed above.

Calculation Procedure

The vorticity and stream-function fields are converged by means of the point SOR technique. New boundary values of the vorticity are calculated as discussed in a previous section. Three conditions must be met before the time step is considered to be converged:

$$(1) \quad E(\psi, k) \leq \epsilon(\psi)$$

$$(2) \quad E(\omega, k) \leq \epsilon(\omega)$$

$$(3) \quad E\left(\frac{\partial\psi}{\partial n}, k\right) \leq \epsilon\left(\frac{\partial\psi}{\partial n}\right)$$

where the terms $E(\psi, k)$, $E(\omega, k)$, and $E\left(\frac{\partial\psi}{\partial n}, k\right)$ are the maximum norms of the change $E(\psi, k) \equiv \|\psi^{(k)} - \psi^{(k-1)}\|_{\infty}$. The terms involving ϵ are simply the required convergence criteria. (Nominal values for $\epsilon(\psi)$, $\epsilon(\omega)$, and $\epsilon\left(\frac{\partial\psi}{\partial n}\right)$ are 10^{-5} , 10^{-5} , and 10^{-2} , respectively.) This procedure is repeated until convergence. Once a time step has converged, time is incremented and the process begins again.

NAVIER-STOKES RESULTS

Solutions About Various Bodies

To illustrate the versatility of the natural coordinate system approach, viscous flows about three different bodies are presented. The bodies and associated flow conditions are

(1) Flapped Kármán-Trefftz airfoil: $\theta = 15^\circ$; $R = 200$

(2) Göttingen 625 airfoil: $\theta = 5^\circ$; $R = 2000$

(3) Cambered rock: $\theta = 5^\circ$; $R = 500$

The coordinates of these bodies are given in reference 4.

Several problems arose with the body vorticity calculations. At times the iterative method used to calculate the body vorticity produced mildly oscillating values along the body boundary. The principal cause of this result was that the method was applied point by point along the boundary. Thus, the only "communication" between the body points was through the field iterations. This tendency was overcome in two ways: First, only small surface vorticity changes were allowed at each body station at each iteration. Second, after the new vorticity values had been calculated, a three-point weighted average was used to smooth the new surface vorticity distribution.

A second problem developed with those bodies having a sharp trailing edge. To preserve continuity of the vorticity, the vorticity at the trailing edge was held at zero. Since the vorticity gradients are extremely large in the neighborhood of the trailing edge, the numerical solution had a tendency to oscillate near this point. This phenomenon is generally known as "wiggles" and, as shown in Roache (ref. 8), is actually the solution of the difference equations. In reality the wiggles are caused by the inability of the net function to resolve large gradients near boundaries.

Flapped Kármán-Trefftz Airfoil

The coordinate system for the flapped Kármán-Trefftz airfoil profile, which possesses a camber of 22 percent at the 0.55-chord point, is shown in figure 5. The free-stream Reynolds number was taken as 200, and the flow angle of attack was 15° . Other data concerning the solution are given in table 1.

Stream-function contours are given for two time steps in figure 11. The contours at the earlier time indicate clearly the large flow velocities over the upper surface of the airfoil and the consequent large difference in overall boundary-layer thickness between the upper and lower surfaces. The manner in which the zero streamline leaves the trailing edge indicates that flow separation on the upper surface is imminent. The contours for $t = 1.06$ illustrate a fully developed laminar separation. The boundary-layer thickness over the aft half of the upper surface has increased approximately 300 percent.

In order to gain some insight into the development of laminar separation, a series of four velocity profiles are shown in figure 12. The profiles for $t = 0.08$ illustrate the upper-surface flow shortly after the impulsive start. The boundary layer is very thin at this time. Separation has already begun at $t = 0.22$, as evidenced by the profiles on the flap portion of the airfoil. Figures 12(c) and 12(d) indicate that the upper-surface separation point has moved rapidly upstream to approximately the 70-percent-chord point. Reverse flow has been well established at $t = 0.54$. Note that the upper-surface boundary-layer thickness has increased substantially over the time span shown.

Göttingen 625 Airfoil

The flow Reynolds number was 2000 at an angle of attack of 5° . Additional summary data of the solution for the Göttingen 625 airfoil appear in table 1. The coordinate system shown in figure 13 was used in this solution. The high density of constant η -lines near the airfoil surface is the result of contraction to the first 15 η -lines. In particular, the amplitude factor appearing in equation (5b) ranged from 20 000 at $\eta = 1$ to 13 000 at $\eta = 15$ (increments of 500/line), while the decay factors were held constant at 1.0 for

$\eta = 1$ to 14 and were 0.4 for the 15th η -line. The function $P(x,y)$ defined by equation (5a) was set to zero as were the point-attraction parameters of equation (5b).

This solution developed wiggles near the sharp trailing edge. The effect of the wiggles is dramatically illustrated in figure 14, which shows ψ and ω contours at several times after the impulsive start. Note the distortion of the vorticity contours near the trailing edge. The oscillatory effects are carried upstream along the lower surface of the airfoil and are proceeding downward, away from the trailing edge. The disturbance proceeds away from the airfoil without much damping but has little effect on the flow in the vicinity of the airfoil after the start, as can be seen in figures 15(a) and (b), which show ψ contours at later times. A feature of interest in figures 14(a) and (b) is the starting vortex which is formed and shed at the trailing edge. This vortex appears just above the disturbance due to the wiggles.

Figure 14(c) indicates that flow separation has been initiated on the trailing-edge portion of the airfoil upper surface. The separation point moves rapidly upstream to approximately the half-chord point at $t = 1.012$. At this time the upstream movement of the separation point slows down considerably. The thickness of the separated region, however, begins to increase, as illustrated in figures 15 and 16. The remainder of the stream-function contours in figures 15(a) and (b) illustrate the growing thickness of the separated region, the increasing back flow, and the separation of flow eddies. At $t = 2.23$ a bubble begins to form on the trailing edge. This bubble continues to grow and is followed by the formation of another bubble at $t = 2.53$. The extent of both bubbles continues to increase until a single bubble is formed at $t = 3.13$. The final ψ contours given indicate that the single bubble has become much larger. The thickness of the separation region is roughly 1.25 times the airfoil thickness at this time, with the forward separation point at approximately 31 percent of the chord.

The separation process may also be examined by viewing the series of upper-surface velocity profiles given in figure 16. The profiles given in figure 16(a) illustrate attached upper-surface flows shortly after the impulsive start. There is a noticeable increase in the boundary-layer thickness at $t = 0.336$. The remaining parts of figure 16 track the growing thickness of the separated region and the upstream movement of the separation point.

Pressure and force coefficients at an early time are illustrated in figure 17(a). The friction drag constitutes more than 65 percent of the total drag at this time. As the boundary layer becomes thicker, the friction drag decreases rapidly and causes a corresponding decrease in the total drag. The effects of the laminar flow separation are shown in figure 17(b). The peculiar variation in the C_p^* distribution at the trailing edge is again due to inaccuracies in the body vorticity distribution.

Cambered Rock

To show that the natural coordinate method could be used with arbitrary shaped bodies, the viscous flow about the cambered rock at a Reynolds number of 500 was developed. The contracted natural coordinate system used in the solution is given in figure 18. The same amplitude and decay factors given for the Göttingen 625 airfoil were used to create this system. Other summary data are presented in table 1.

With a body such as the cambered rock, reliance must be placed on one's physical intuition in evaluating the resulting flow. For this reason an extended discussion of the flow past the cambered rock will not be given. Instead a significant number of ψ and ω contours will be given. These are shown in figure 19. However, it is felt that some remarks are appropriate. A glance at figure 18 indicates that the rock possesses several concave areas. Intuition would imply that flow stagnation areas should develop quite rapidly in these regions. This, in fact, does occur, as figure 19 indicates. In addition one would expect laminar flow separation and the consequent shedding of vorticity from the body. These events are also borne out by the contours. The ever-increasing size of the region of significant vorticity is quite apparent from the figures. Finally, velocity profiles and surface pressure distributions are shown in figures 20 and 21.

Computer Time Requirements

Numerical solutions to parabolic partial differential equations require extensive amounts of digital computer time. The total CPU times (UNIVAC 1106) used to generate the three solutions discussed in this study are documented in table 1. The average time required to converge each time step is also shown. (No attempt was made to quantify the effects of time-step size on the average times given.)

CONCLUSIONS

The objective of this study was to develop methods to obtain numerical solutions of the two-dimensional, incompressible, time-dependent Navier-Stokes equations about arbitrary bodies. The solutions followed the development of a general numerical curvilinear coordinate transformation which produces a natural coordinate system having a constant coordinate line coincident with each boundary contour in the physical plane. Once the natural coordinates are developed for a given physical domain, the set of partial differential equations of interest may be transformed to the natural system and solved numerically in the transformed plane without regard to the geometry of the physical region. In effect the natural coordinate method eliminates all geometrical considerations from a given solution, as all physical regions have the same appearance in the transformed plane. The computer software utilized to generate the natural coordinates

is independent of the set of partial differential equations whose solution is to be carried out on the transformed plane. The partial differential equations governing potential and viscous flow differ drastically. However, for a given body geometry, the same natural system was used herein for both solutions. The second major advantage of using natural coordinates is that the computer software generated to approximate the solution of a given set of partial differential equations is completely independent of the physical geometry of the problem. The same computer program was utilized to develop all the solutions for the wide variety of bodies discussed herein. Only the input varies with the body. Such a procedure obviously has significant ramifications in numerical mathematics and all areas of physical science.

Significant viscous-flow results were obtained for three different bodies. These included two general airfoil sections and one completely arbitrary body. The airfoil solutions developed computational wiggles near the sharp trailing edge at the start of the impulsive flow. The wiggles were generated as a result of large vorticity gradients which appeared in this region at the start. This disturbance was convected away from the body essentially undamped, but produced no significant disturbance near the body at later times. The solutions show the formation and development of the boundary layer, laminar separation bubbles, and completely separated flow. Present results extend to a Reynolds number of 2000. Although the magnitude of the calculated force coefficients cannot be compared with experimental data, as none exist at this low Reynolds number, the time variation of these parameters agreed quite well with the flow pattern development. The cambered-rock solution proved that the natural coordinate methods could be applied to very general bodies. The manner of this flow development also agreed with intuitive physical reasoning.

There appears to be no basic barrier to higher Reynolds number solutions, since the means are at hand to contract the coordinate system about the body as much as desired. Preliminary runs at a Reynolds number of 10 000 have already been made. Work is also in progress on the solution for multiple airfoils with viscous flow.

REFERENCES

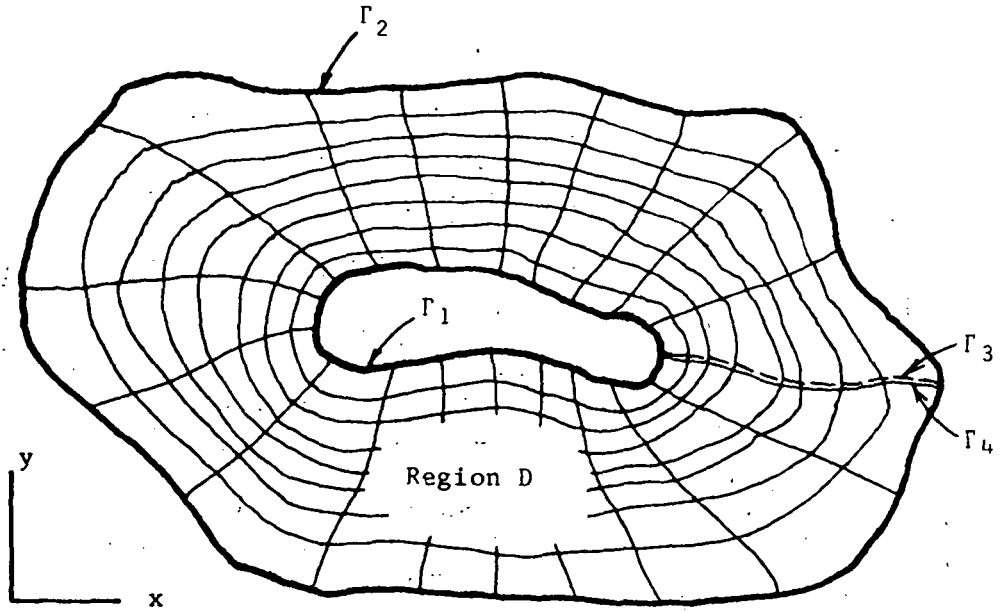
1. Mehta, U. B.; and Lavan, Z.: Starting Vortex, Separation Bubbles and Stall - A Numerical Study of Laminar Unsteady Flow Around an Airfoil. AFOSR-TR-73-0640, Dec. 1972. (Available from DDC as AD 758 831.)
2. Dawson, C.; and Marcus, M.: DMC - A Computer Code To Simulate Viscous Flow About Arbitrary Shaped Bodies. Proceedings of the 1970 Heat Transfer and Fluid Mechanics Institute, 1970, pp. 323-338.
3. Thompson, Joe F.; Thames, Frank C.; and Mastin, C. Wayne: Automatic Numerical Generation of Body-Fitted Curvilinear Coordinate System for Field Containing Any Number of Arbitrary Two-Dimensional Bodies. J. Computational Phys., vol. 15, no. 3, July 1974, pp. 299-319.
4. Thames, Frank C.: Numerical Solution of the Incompressible Navier-Stokes Equations About Arbitrary Two-Dimensional Bodies. Ph. D. Diss., Mississippi State University, 1975.
5. Giesing, Joseph P.: Potential Flow About Two-Dimensional Airfoils. Part I: A Summary of Two-Dimensional Airfoil Methods; Part II: Solution of the Flow Field About One or More Airfoils of Arbitrary Shape in Uniform or Nonuniform Flows by the Douglas Neumann Method. Rep. No. LB31946, Douglas Aircraft Co., Inc., Dec. 1, 1965.
6. Karamcheti, Krishnamurty: Principles of Ideal-Fluid Aerodynamics. John Wiley & Sons, Inc., 1966.
7. Liebeck, Robert H.: A Class of Airfoils Designed for High Lift in Incompressible Flow. AIAA Paper No. 73-86, Jan. 1973.
8. Roache, Patrick J.: Computational Fluid Dynamics. Hermosa Publ., c.1972.
9. Israeli, M.: A Fast Implicit Numerical Method for Time-Dependent Viscous Flows. Studies in Appl. Math, vol. 49, 1970, p. 327.
10. Ortega, J. M.; and Rheinboldt, W. C.: Iterative Solution of Nonlinear Equations in Several Variables. Academic Press, Inc., 1970.

TABLE 1.- SUMMARY OF DATA FOR VISCOUS-FLOW SOLUTIONS

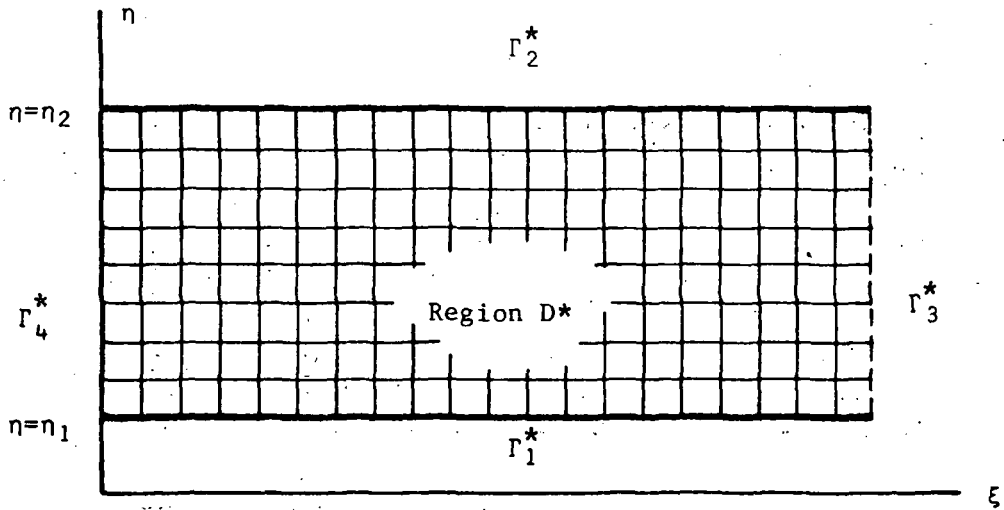
Body (*)	θ , deg	R	Field size	Convergence criteria			Time steps		Average number of iterations		Total solution time	Total CPU time, hr
				ψ	ω	$\frac{\partial\psi}{\partial n}$	Initial	Final	Initial	Final		
1	15	200	3828 (66 × 58)	10 ⁻⁵	10 ⁻⁵	10 ⁻²	0.01	0.03	280	280	1.15	7.104
2	5	2000	4350 (75 × 58)	10 ⁻⁵	10 ⁻⁵	10 ⁻¹	.001	.01	130	220	3.35	32.40
3	5	500	3132 (54 × 58)	10 ⁻⁵	10 ⁻⁵	0.5	.005	.005	55	95	1.30	6.40

*Body code:

- 1 Flapped Kármán-Trefftz airfoil
- 2 Göttingen 625 airfoil
- 3 Cambered rock

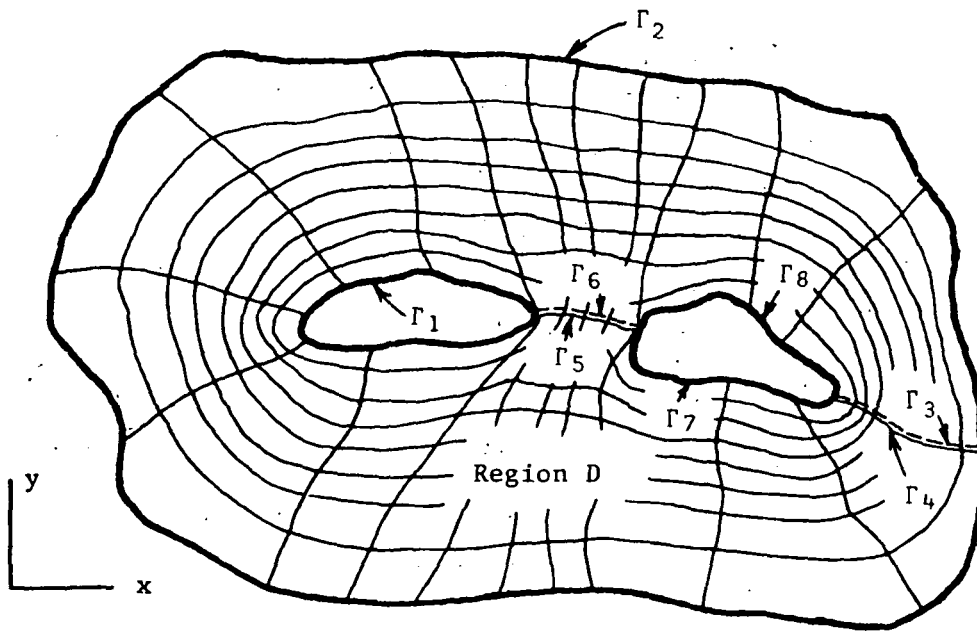


Physical Plane

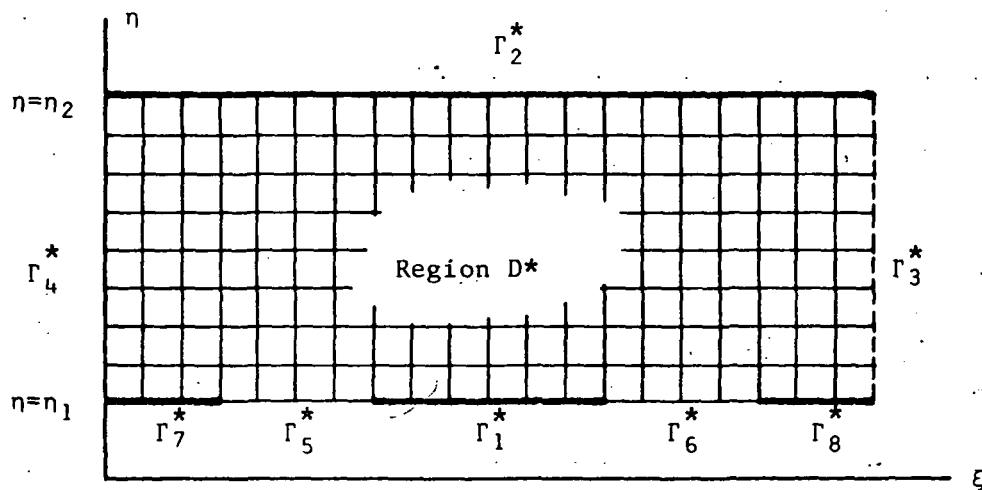


Transformed Plane
(Natural Coordinates)

Figure 1.- Field transformation - single body.

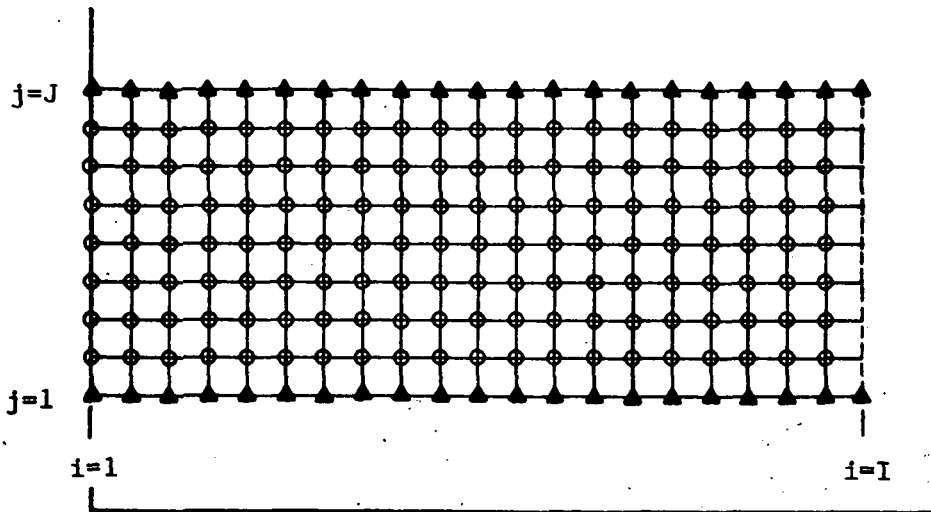


Physical Plane

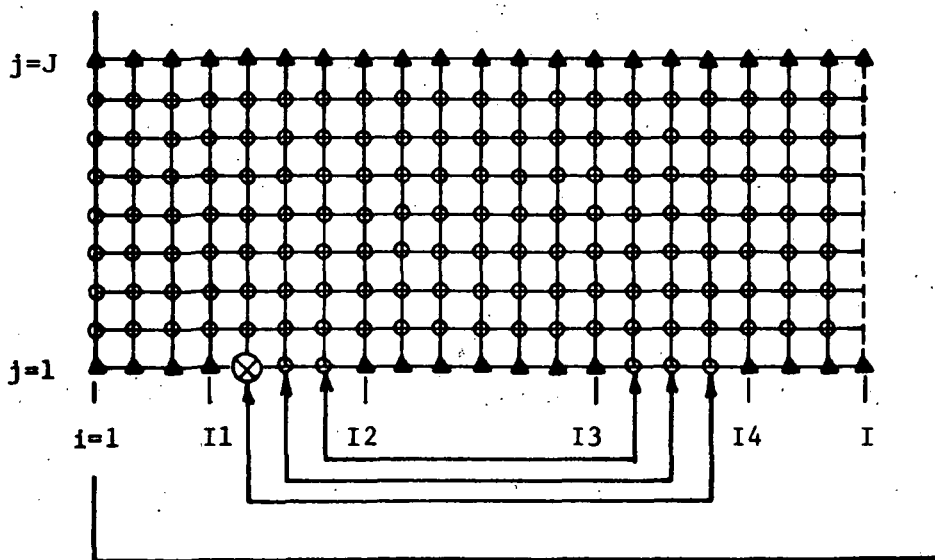


Transformed Plane

Figure 2.- Field transformation - multiple bodies.



(a) Single-body region.



(b) Two-body region.

Figure 3.- Computational grids - single and two-body regions.

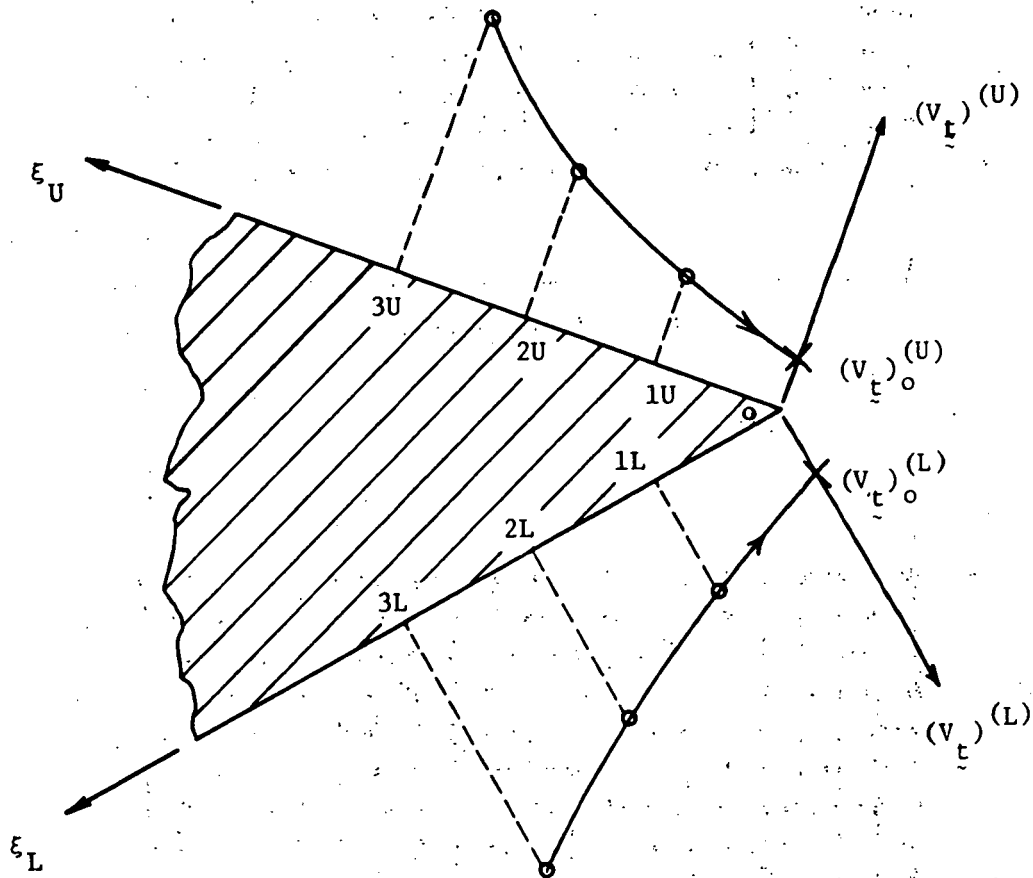


Figure 4.- Velocity extrapolation at airfoil trailing edge.

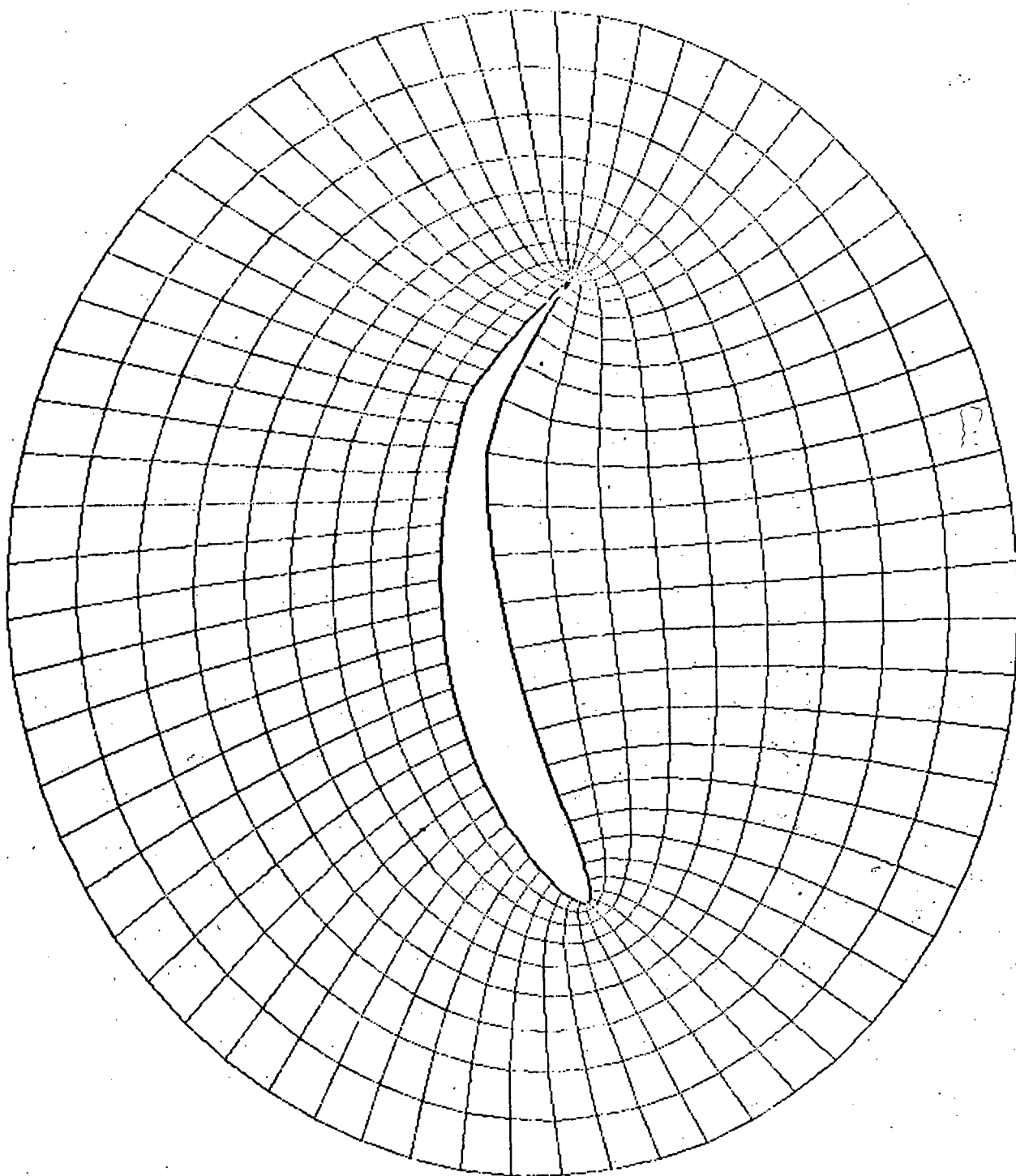


Figure 5.- Coordinate system for flapped Kármán-Trefftz airfoil.

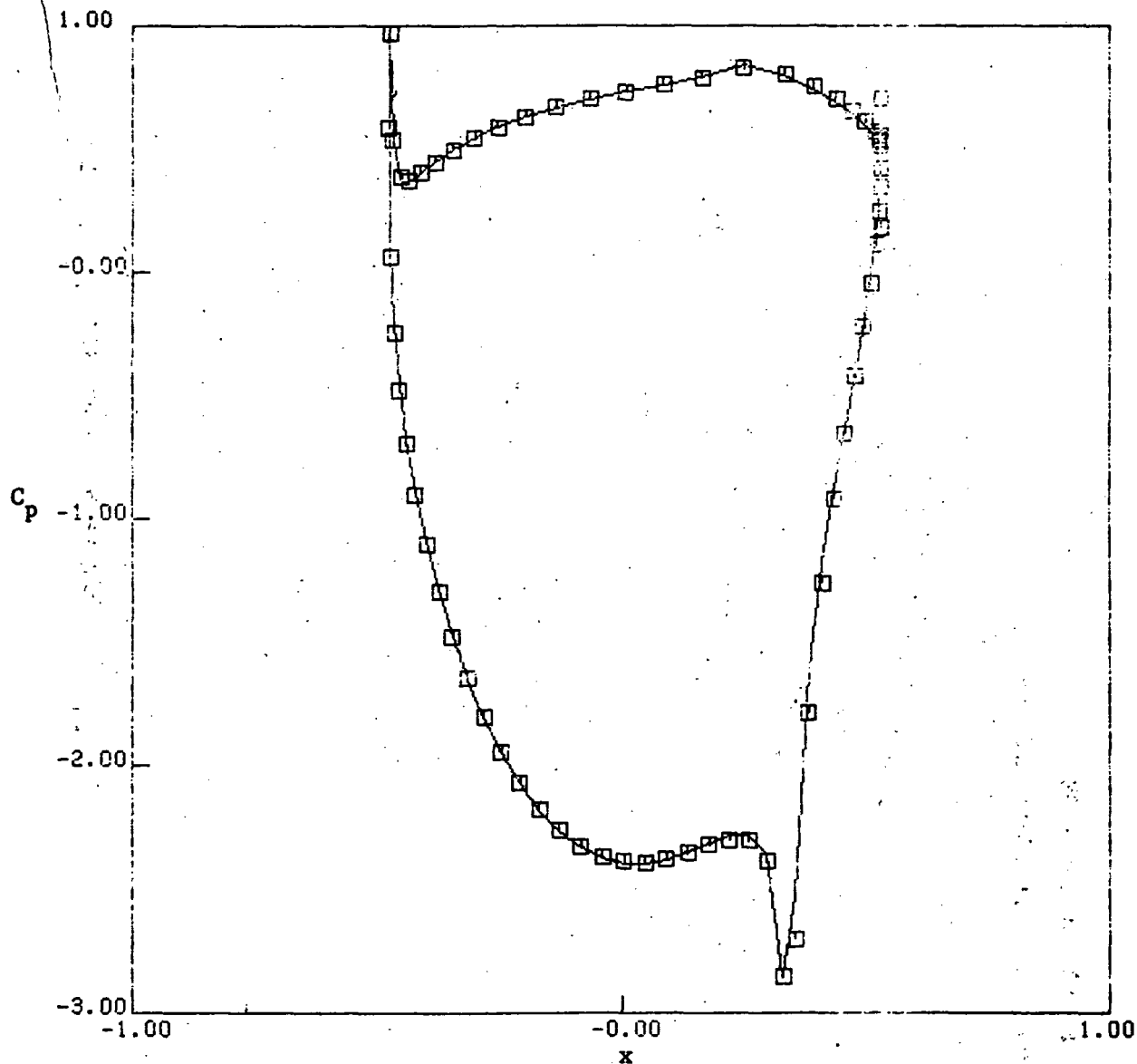
LIFT COEFFICIENT = 2.538680

□ NUMERICAL SOLUTION

DRAG COEFFICIENT = 0.004002

— ANALYTIC SOLUTION(REF.6)

LIFT COEFFICIENT ERROR = -0.001917

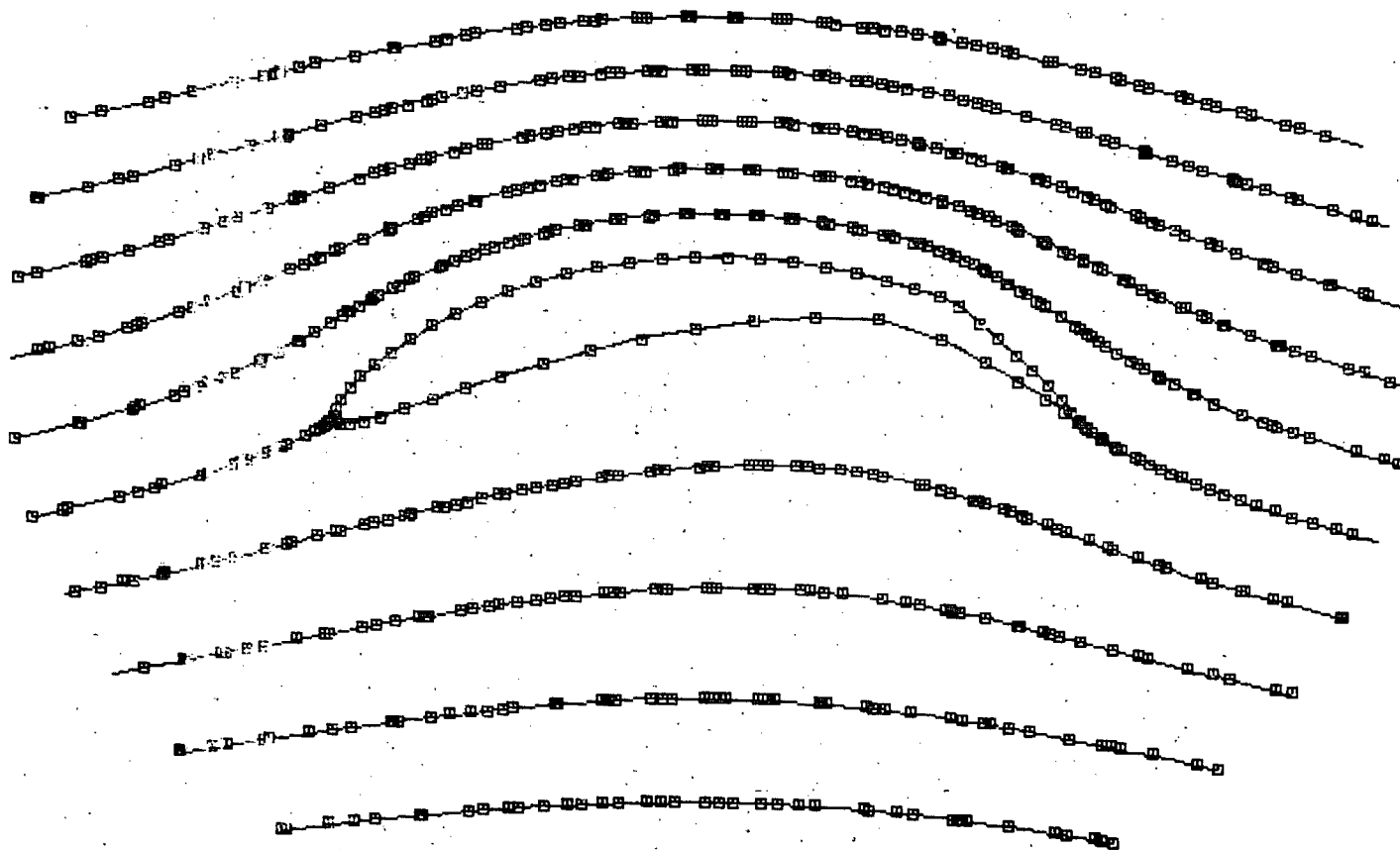


(a) Pressure distribution.

Figure 6.- Analytic and numerical potential-flow results for flapped Kármán-Trefftz airfoil.

□ NUMERICAL SOLUTION

— ANALYTIC SOLUTION(REF. 6)



(b) Streamlines.

Figure 6.- Concluded.

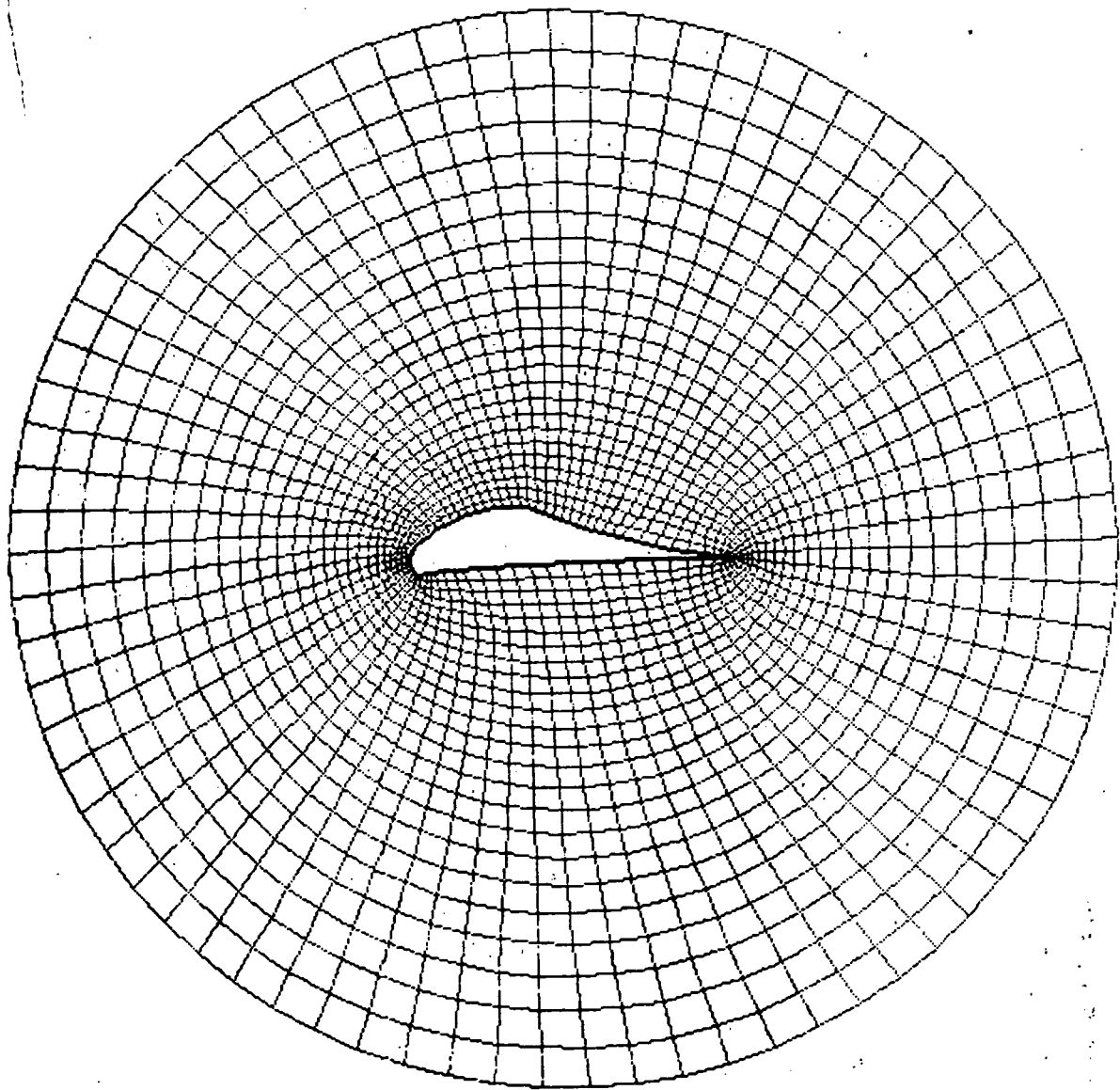
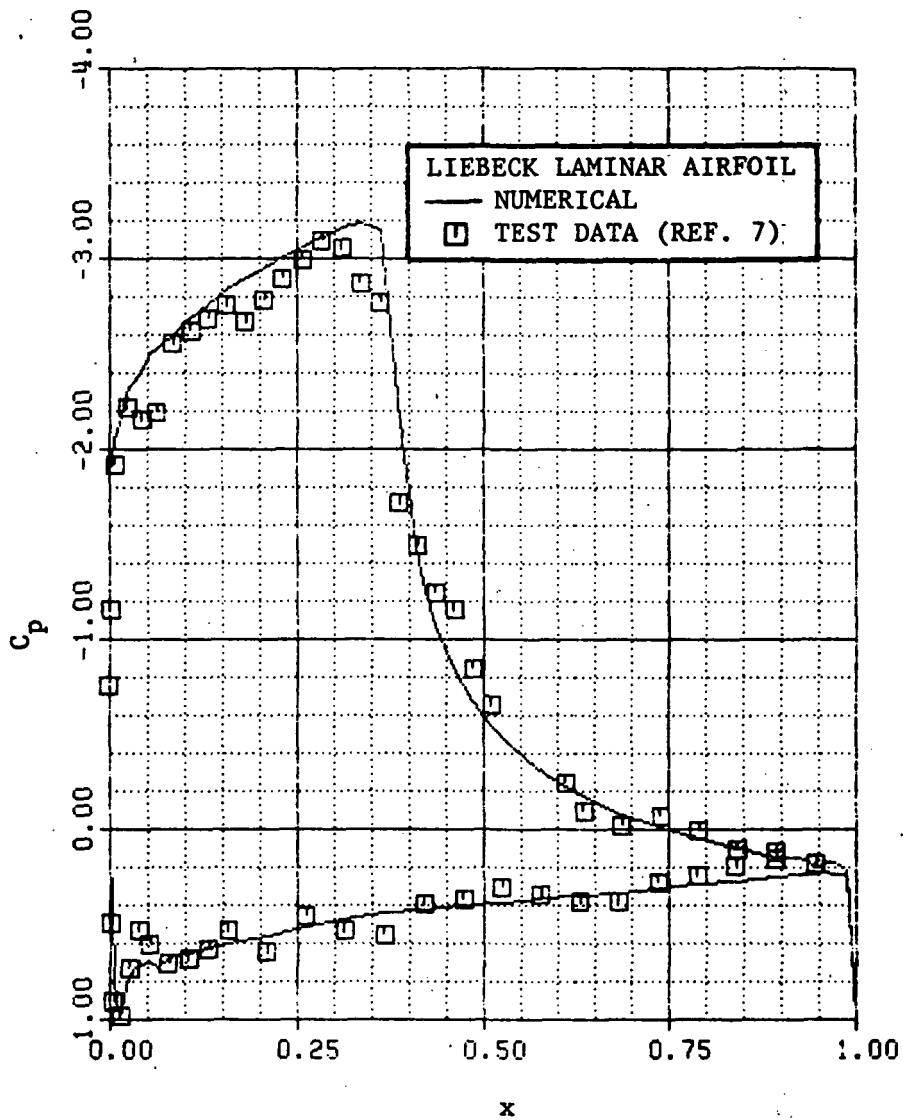


Figure 7.- Coordinate system for Liebeck laminar airfoil.

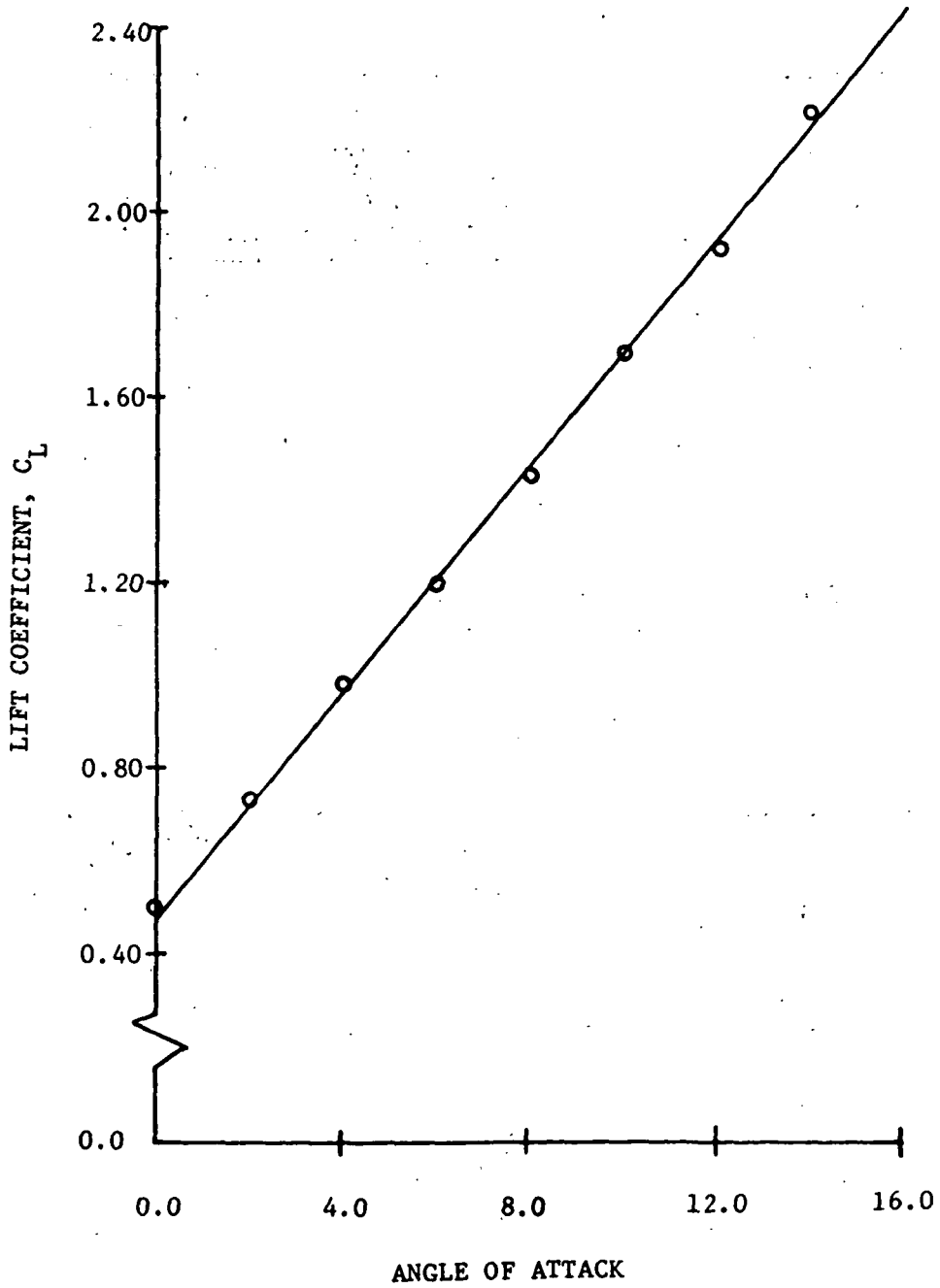


(a) Pressure distribution.

Figure 8.- Experimental and numerical potential-flow results for Liebeck laminar airfoil.

LIEBECK LAMINAR AIRFOIL

— NUMERICAL
○ TEST DATA (REF. 7)



ANGLE OF ATTACK

(b) Lift curve.

Figure 8.- Concluded.

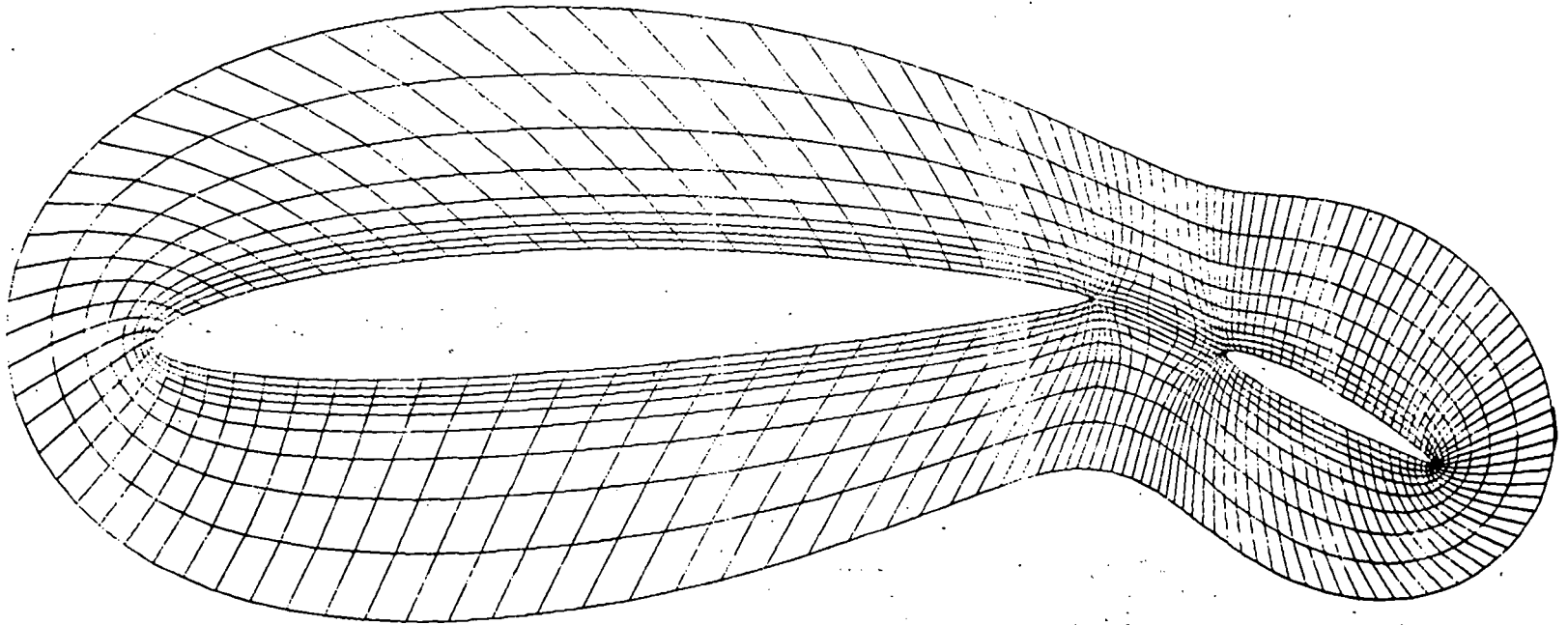
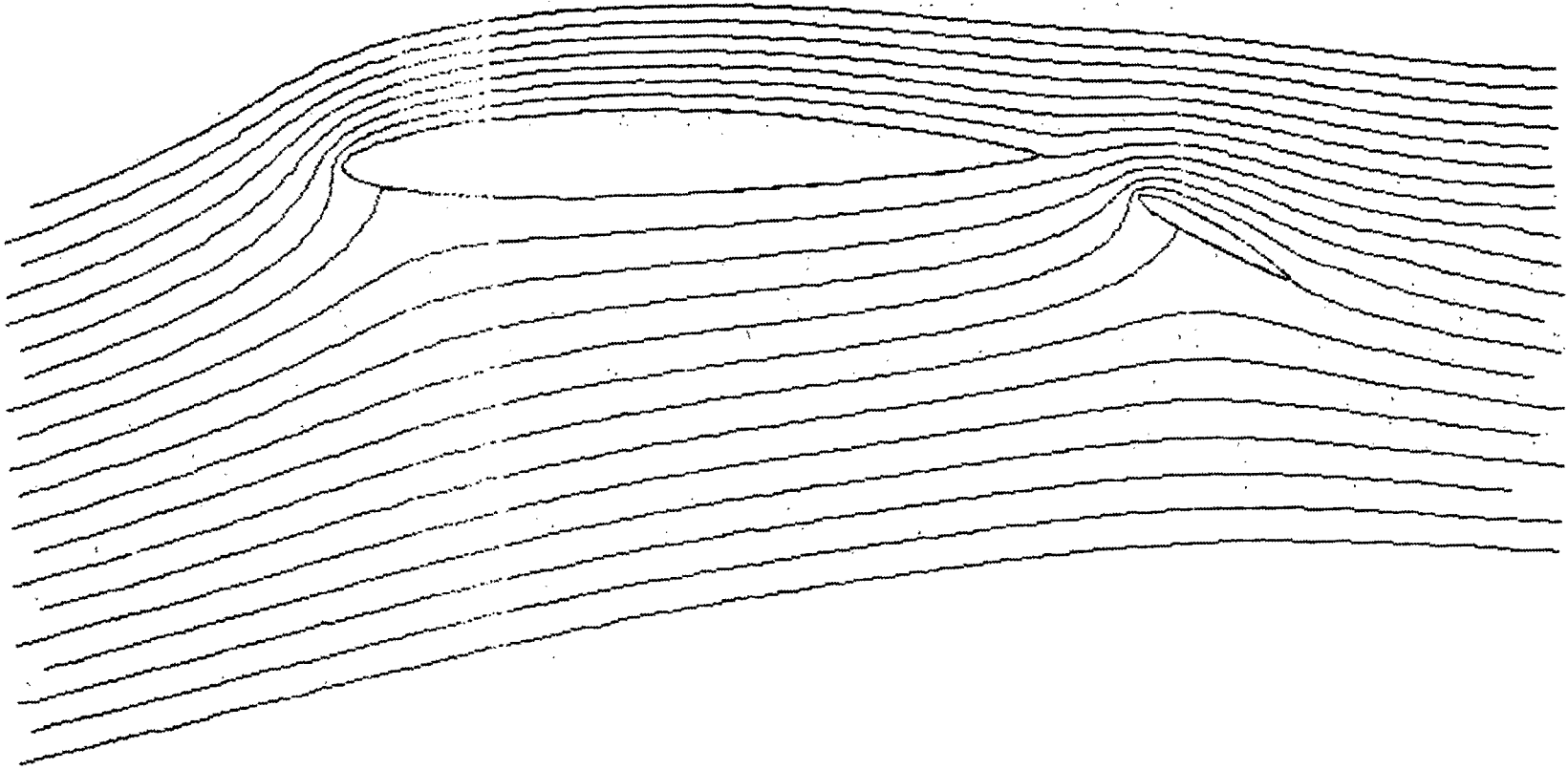
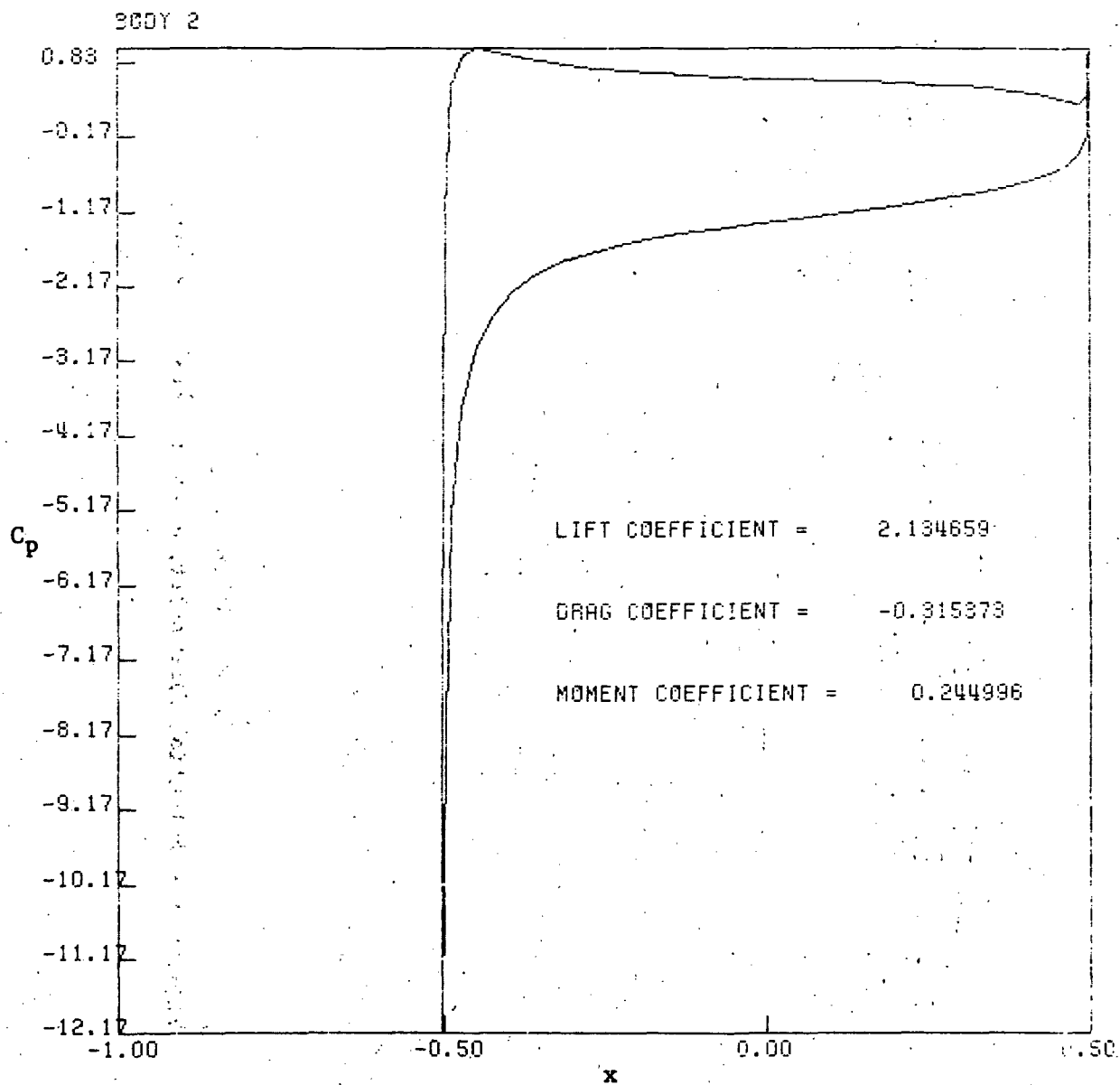


Figure 9.- Coordinate system for multiple airfoil.



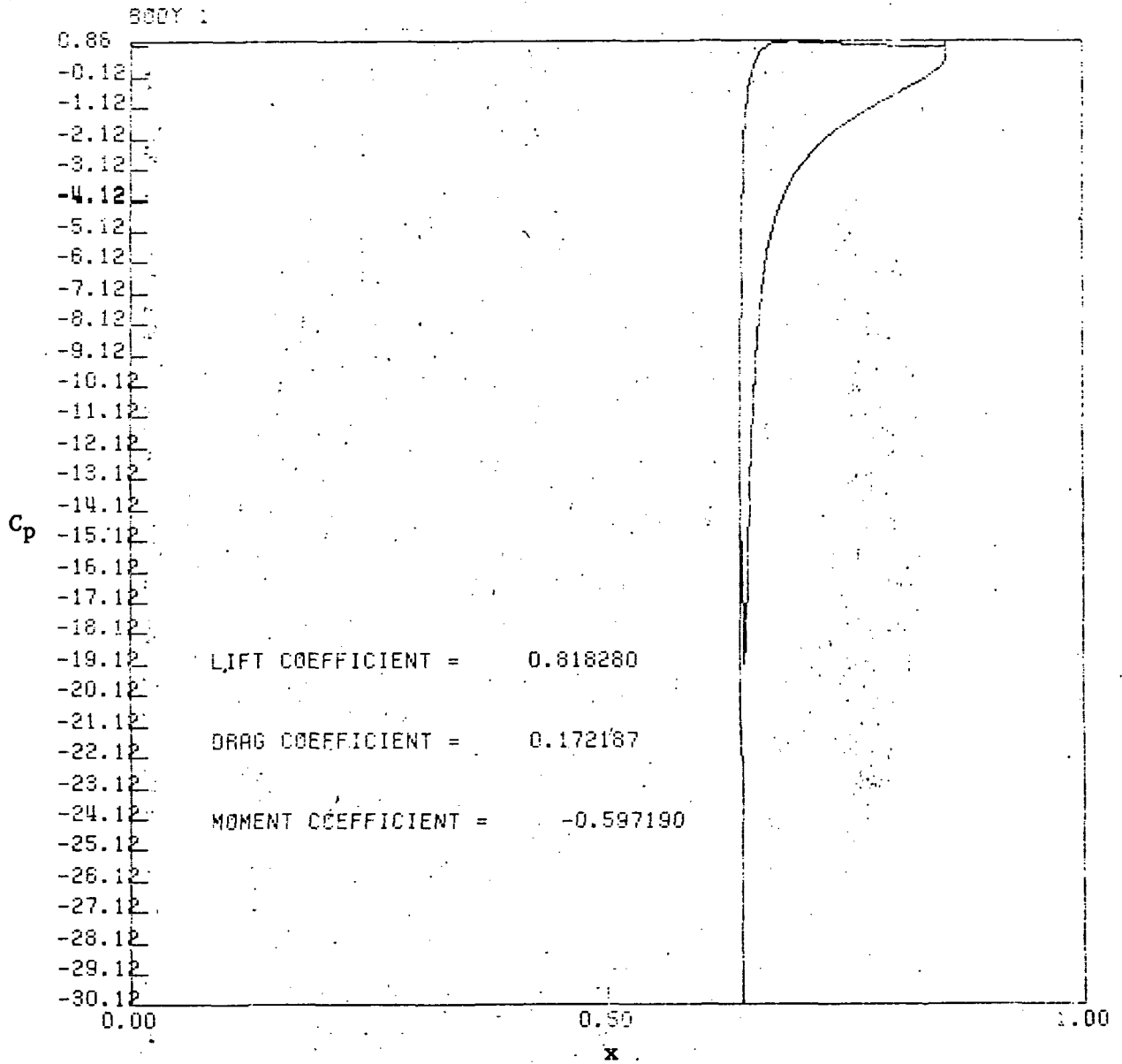
(a) Streamlines.

Figure 10.- Potential-flow solution for multiple airfoil.



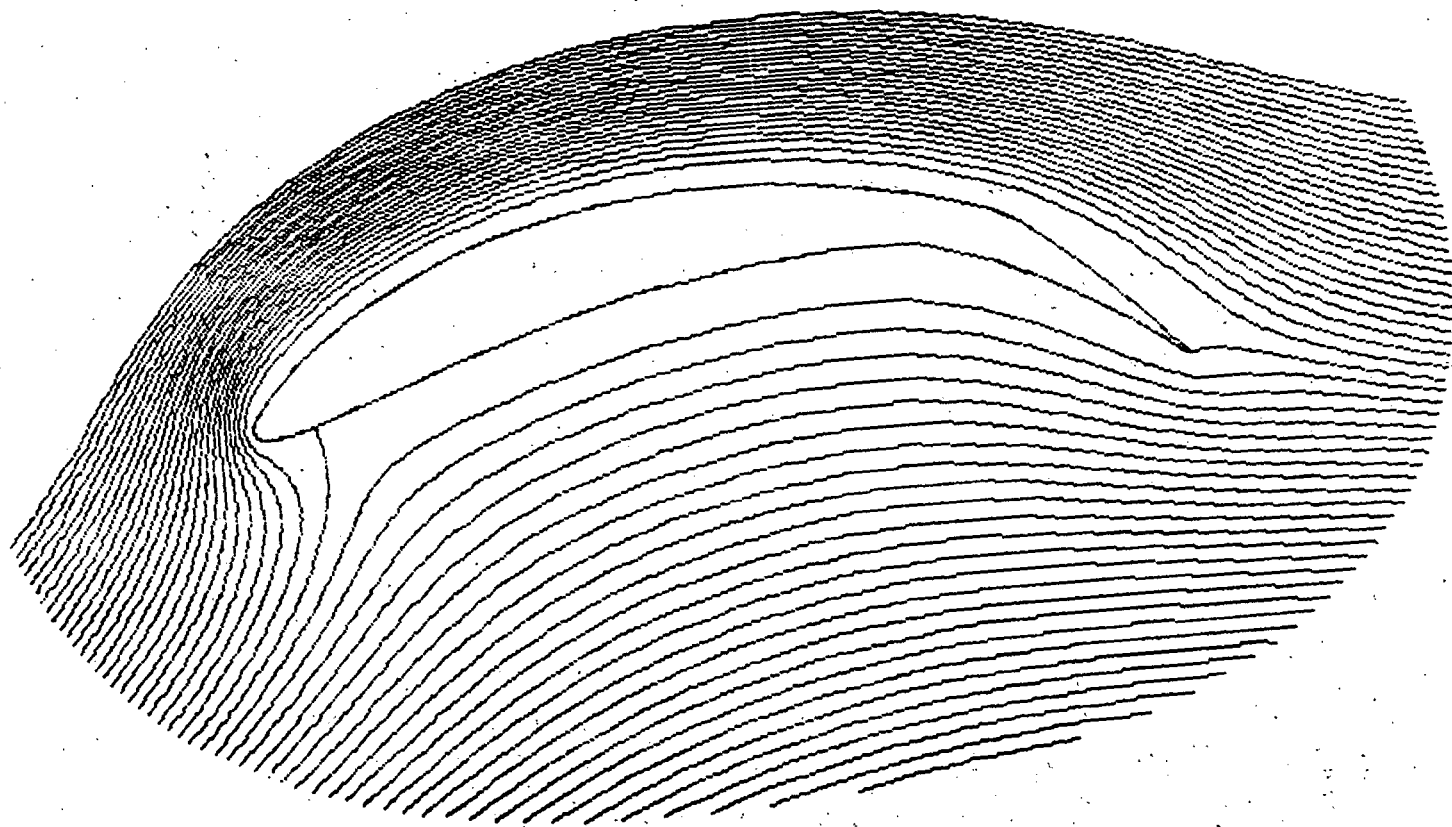
(b) Pressure distribution - fore body.

Figure 10.- Continued.



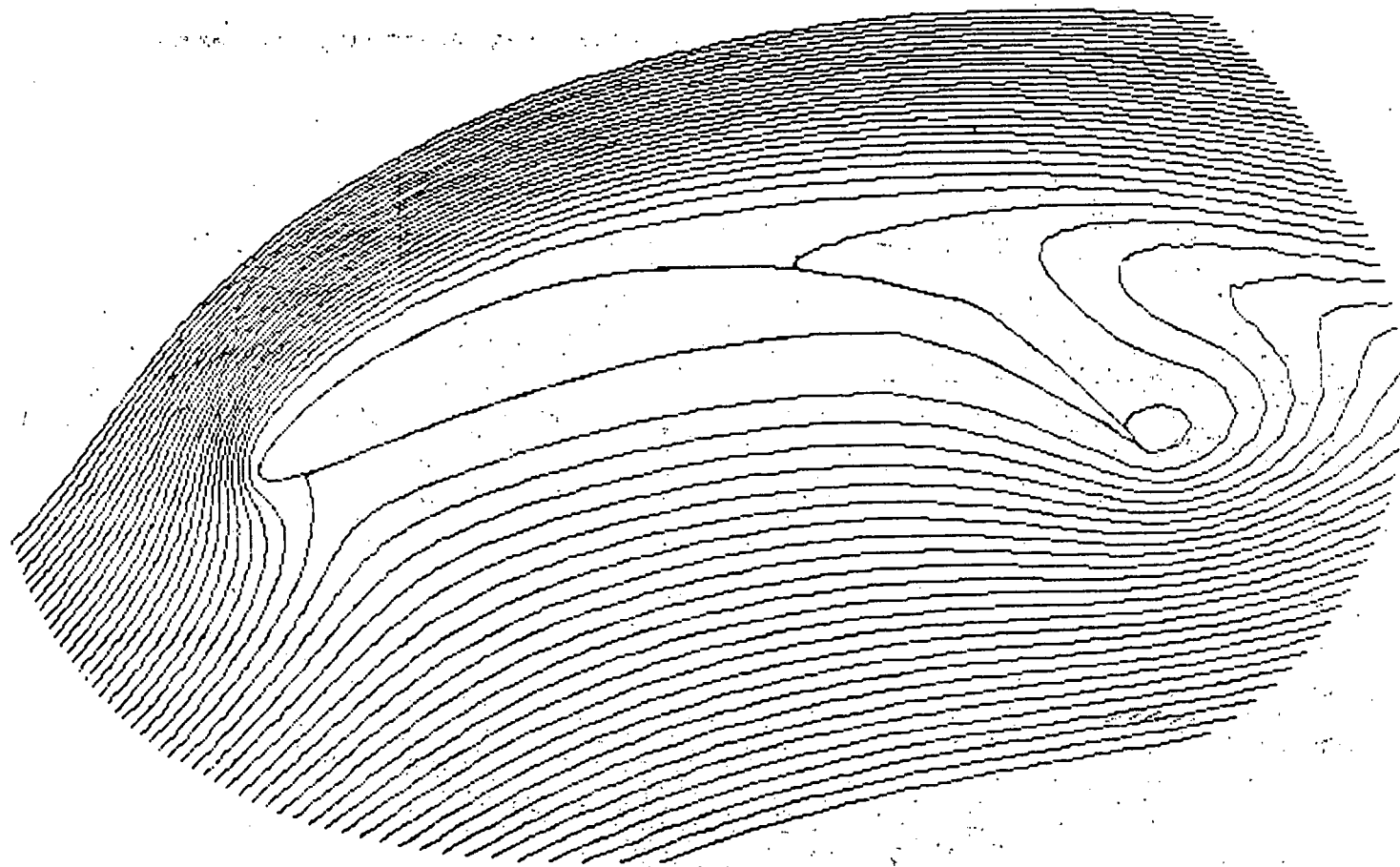
(c) Pressure distribution - aft body.

Figure 10.- Concluded.



(a) $t = 0.22$.

Figure 11.- Stream-function contours for flapped Kármán-Trefftz airfoil.



(b) $t = 1.06$.

Figure 11.- Concluded.

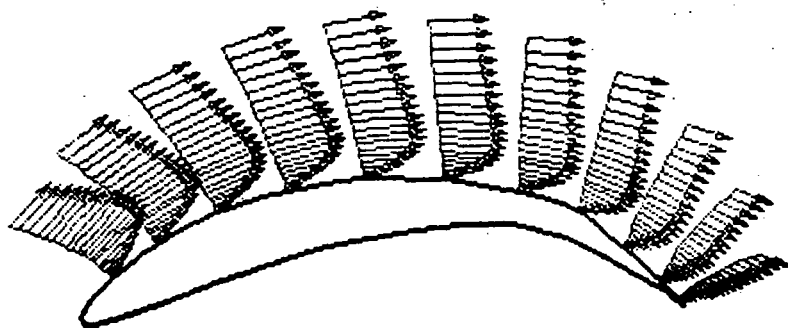
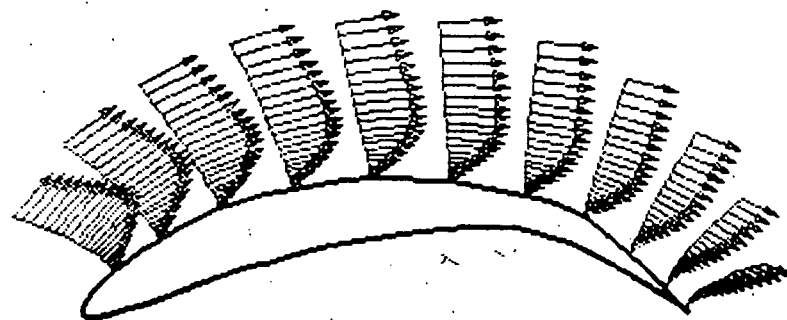
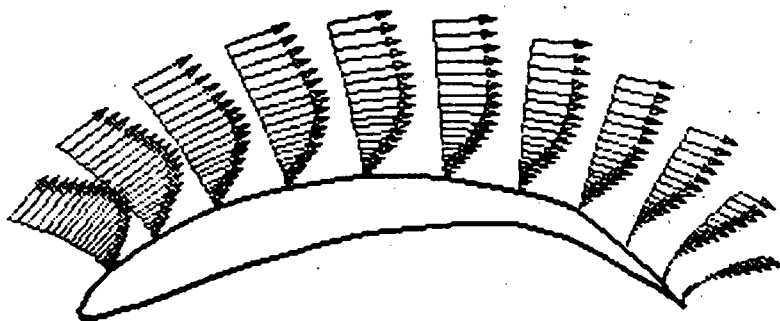
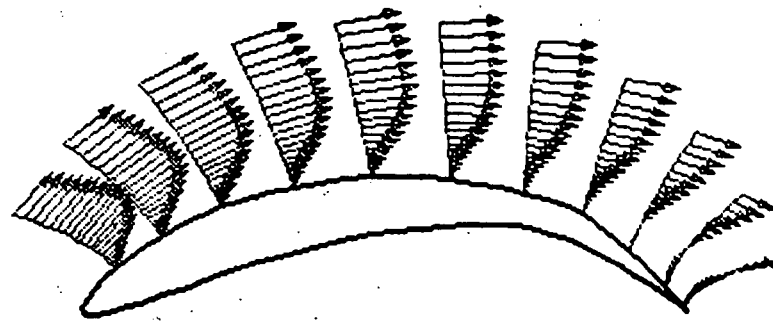
(a) $t = 0.08.$ (b) $t = 0.22.$ (c) $t = 0.38.$ (d) $t = 0.54.$

Figure 12.- Velocity profiles for flapped Kármán-Trefftz airfoil.

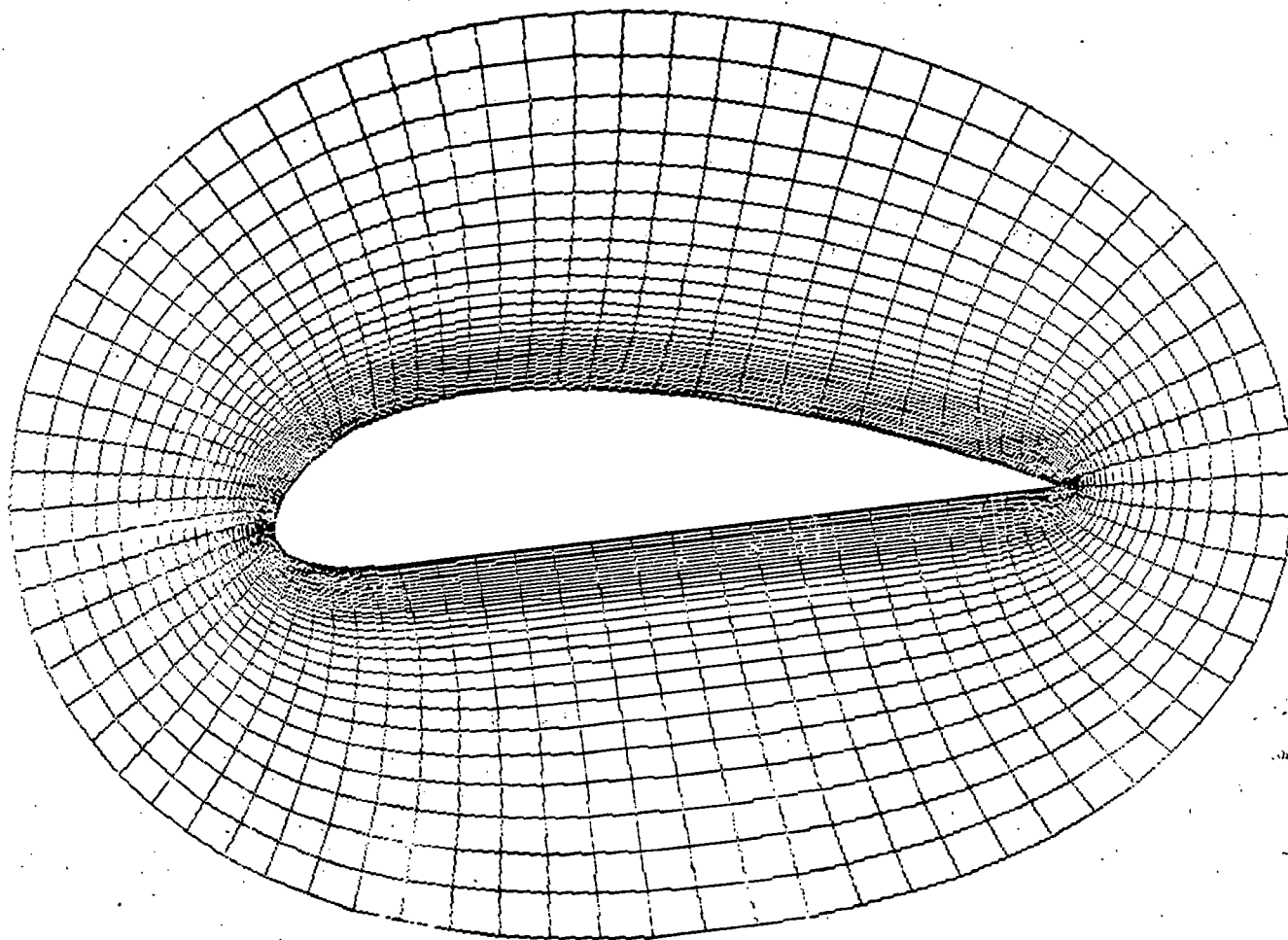
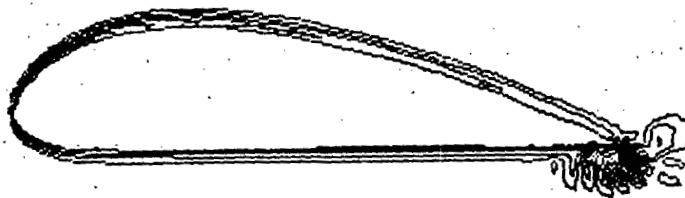
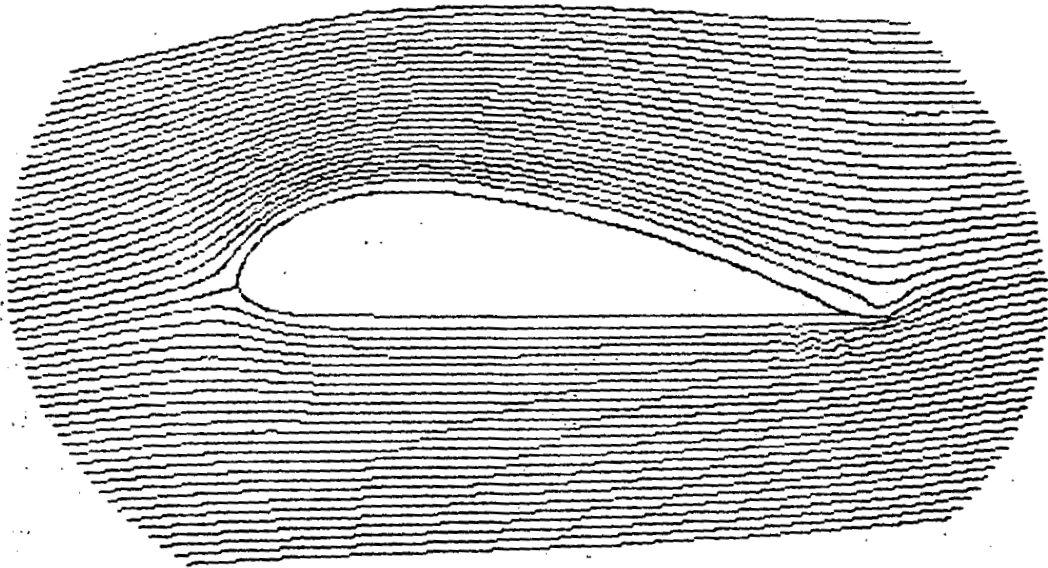
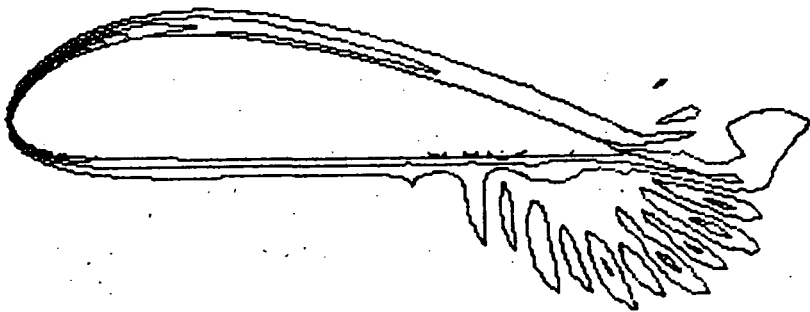
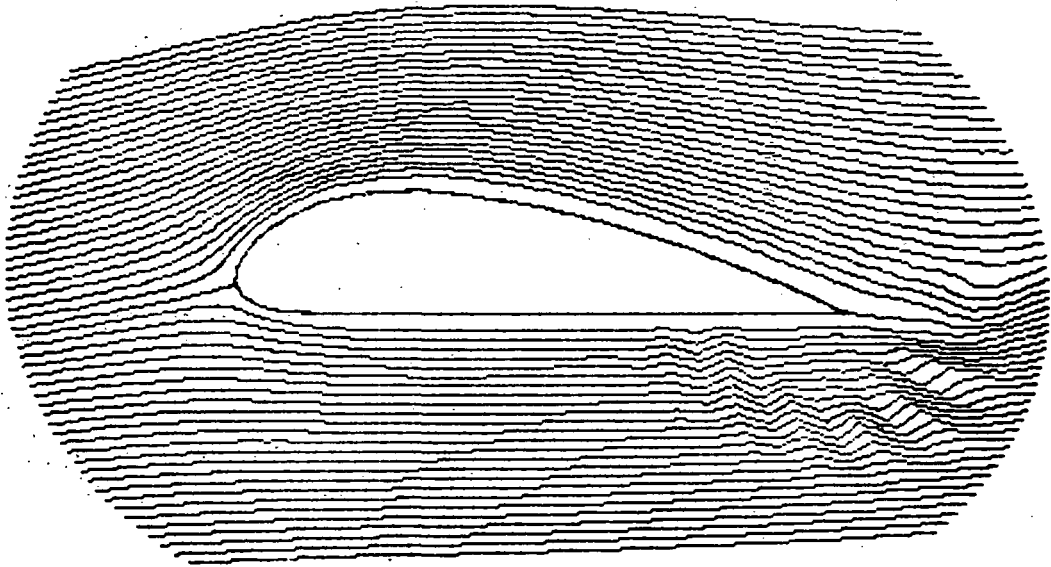


Figure 13.- Contracted coordinate system for the Göttingen 625 airfoil.



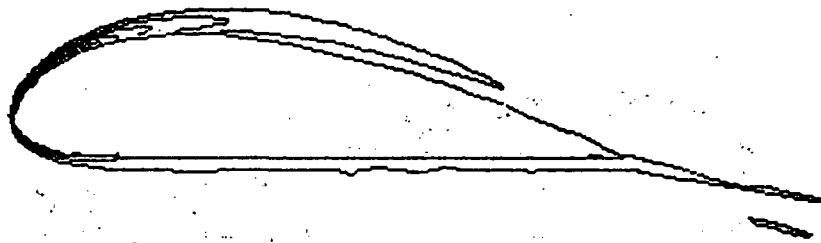
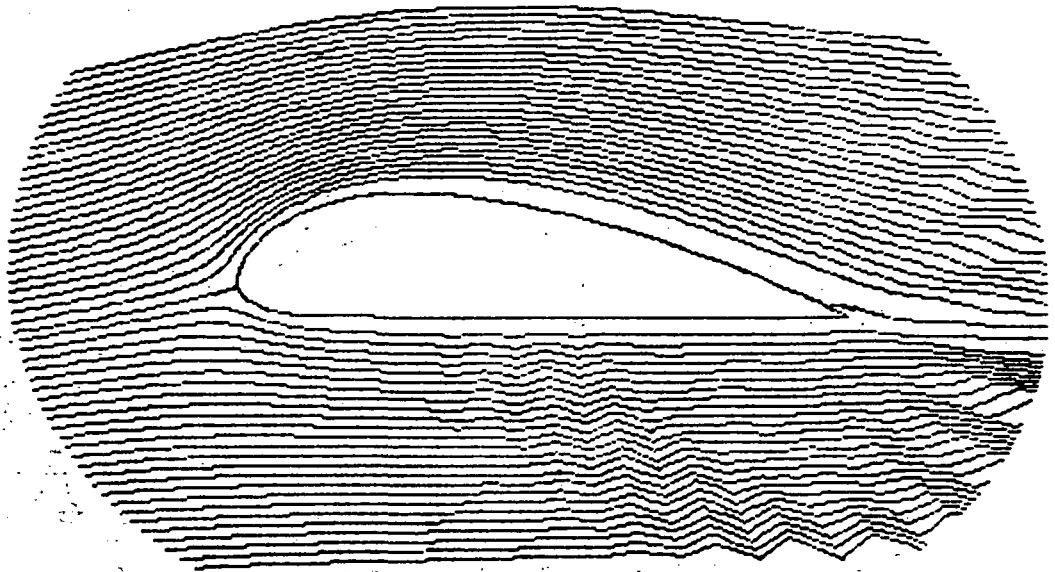
(a) $t = 0.118$.

Figure 14.- Stream-function and vorticity contours for Göttingen 625 airfoil.



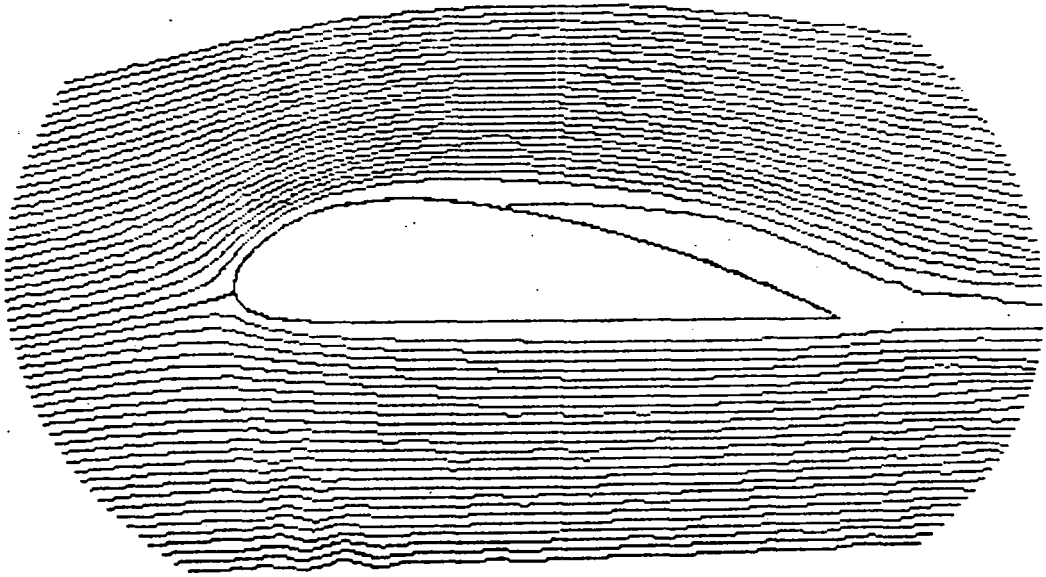
(b) $\tau = 0.336$.

Figure 14.- Continued.

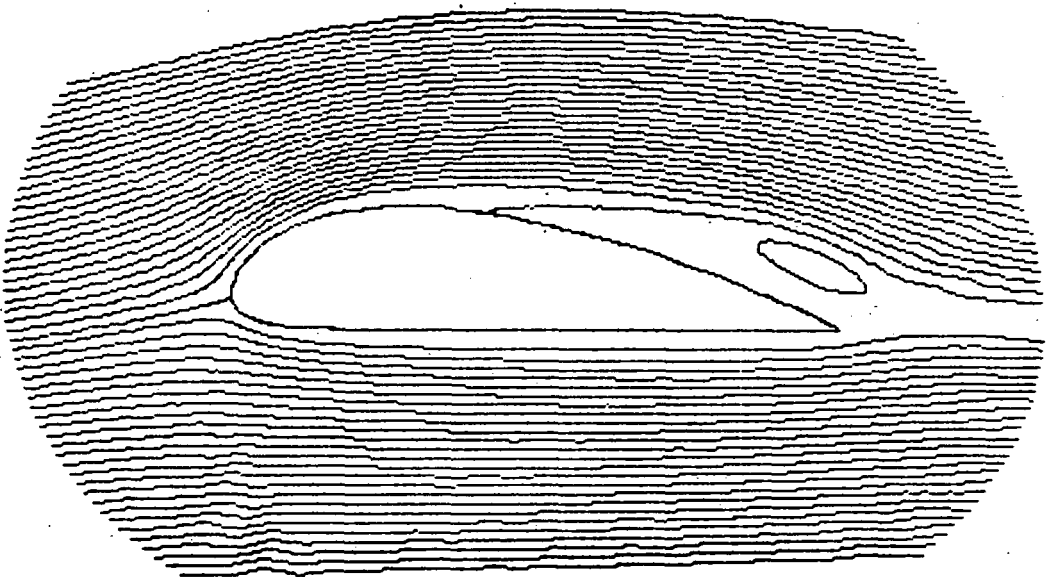


(c) $t = 0.658$.

Figure 14.- Concluded.



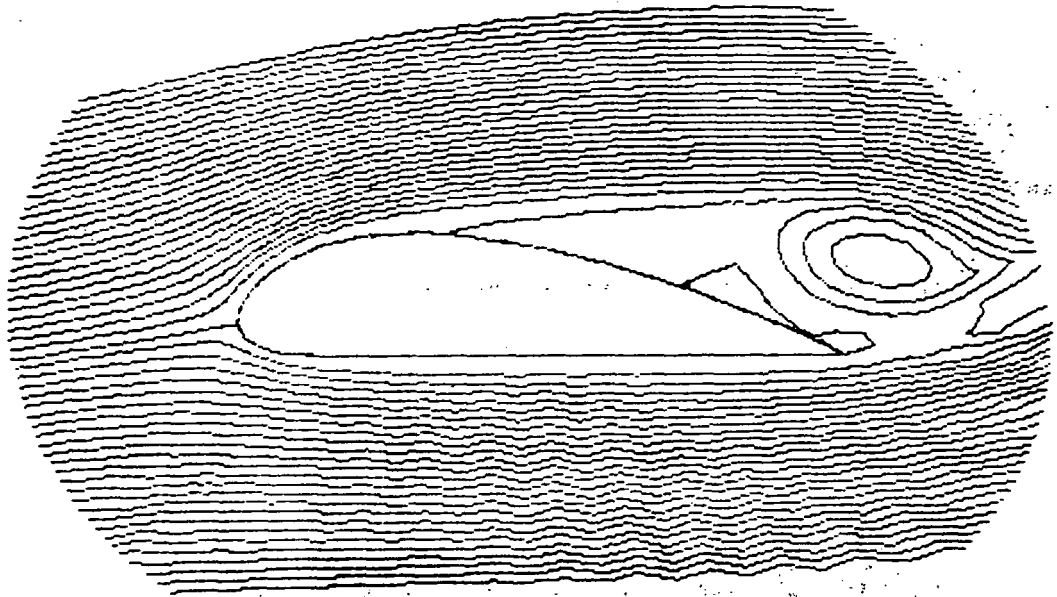
$t=1.53$



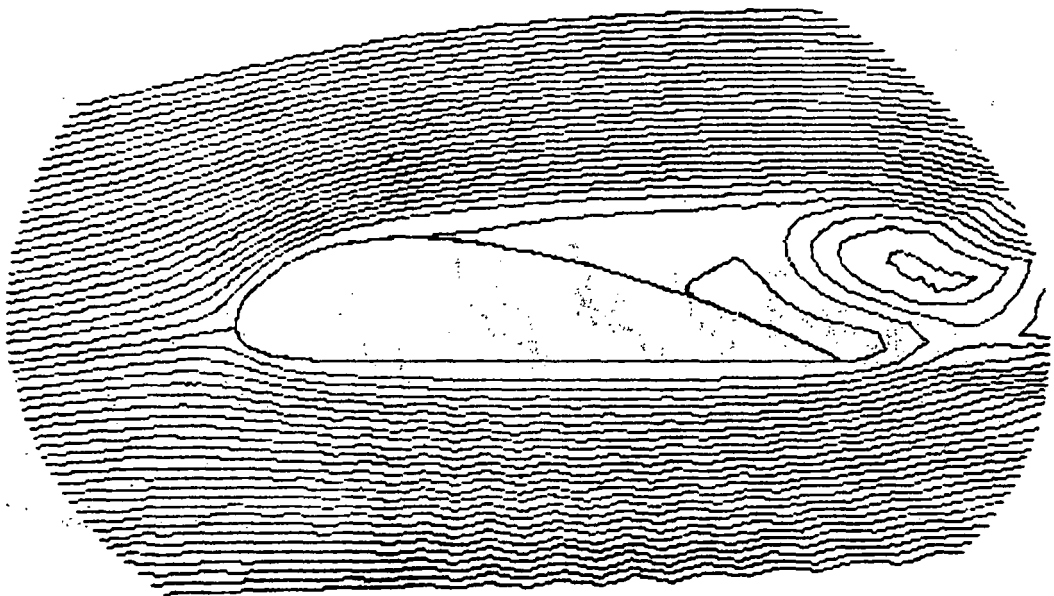
$t=1.83$

(a) $t = 1.53$ and 1.83 .

Figure 15.- Stream-function contours for Göttingen 625 airfoil.



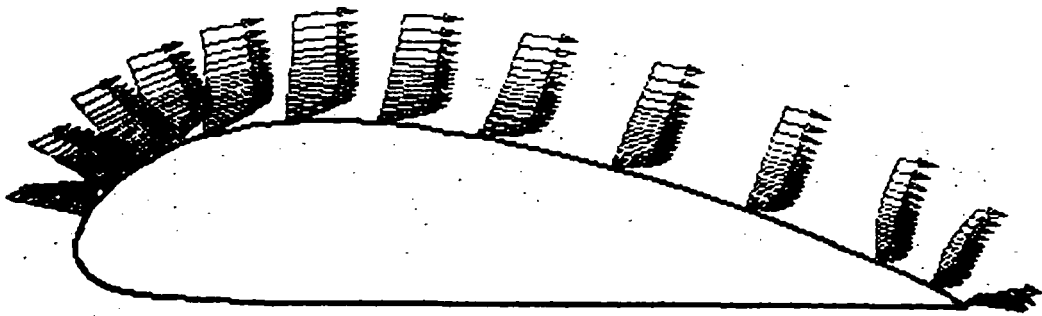
t=3.13



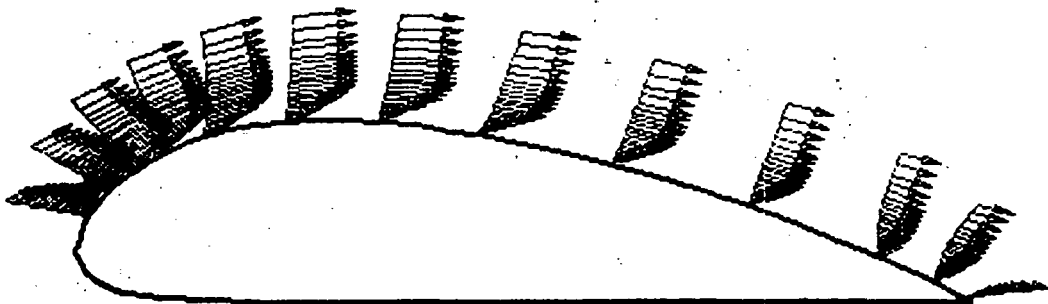
t=3.33

(b) $t = 3.13$ and 3.33 .

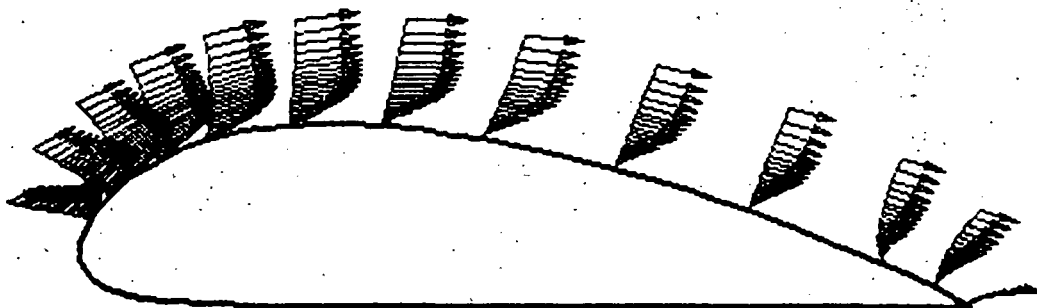
Figure 15.- Concluded.



$t=0.118$



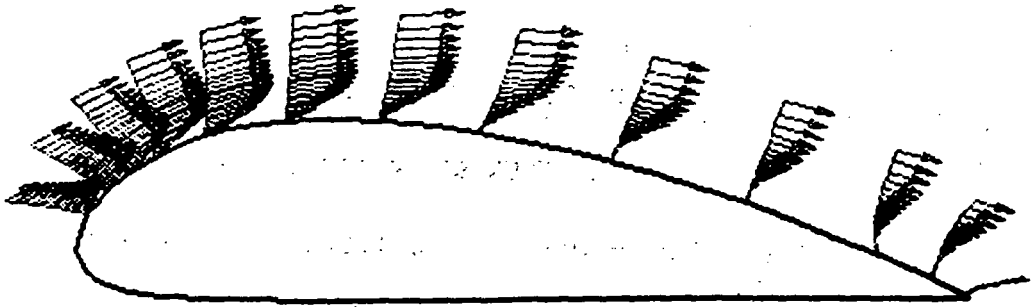
$t=0.336$



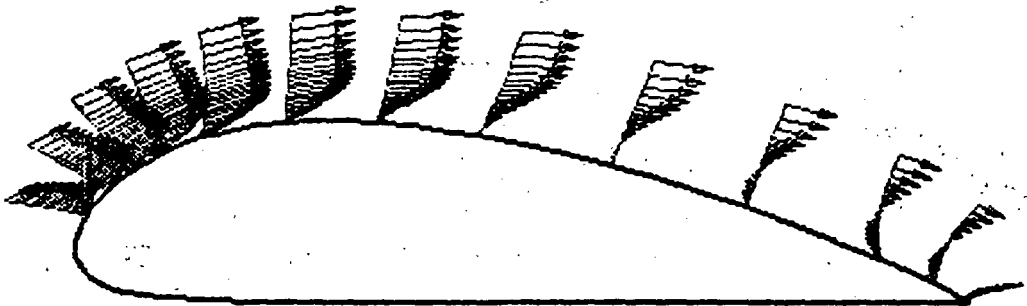
$t=0.658$

(a) $t = 0.118, 0.336, \text{ and } 0.658.$

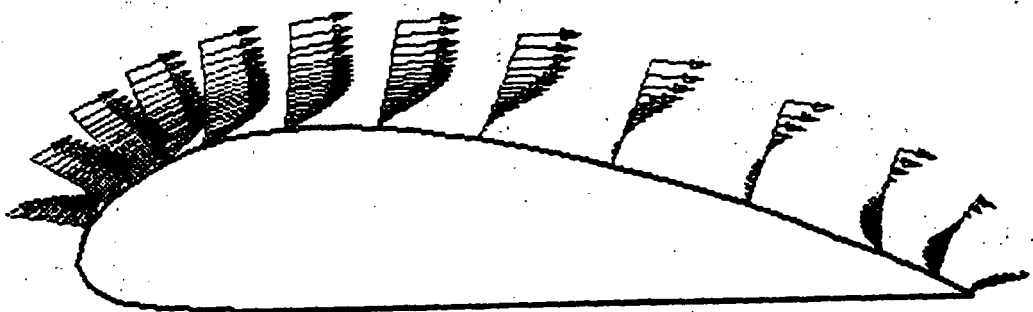
Figure 16.- Upper-surface velocity profiles for Göttingen 625 airfoil.



$t=1.012$



$t=1.53$



$t=1.83$

(b) $t = 1.012, 1.53, \text{ and } 1.83.$

Figure 16.- Concluded.

PRESSURE DISTRIBUTION

GÖTTINGEN 625 AIRFOIL

ANGLE OF ATTACK=5.00

REYNOLDS NUMBER=2000

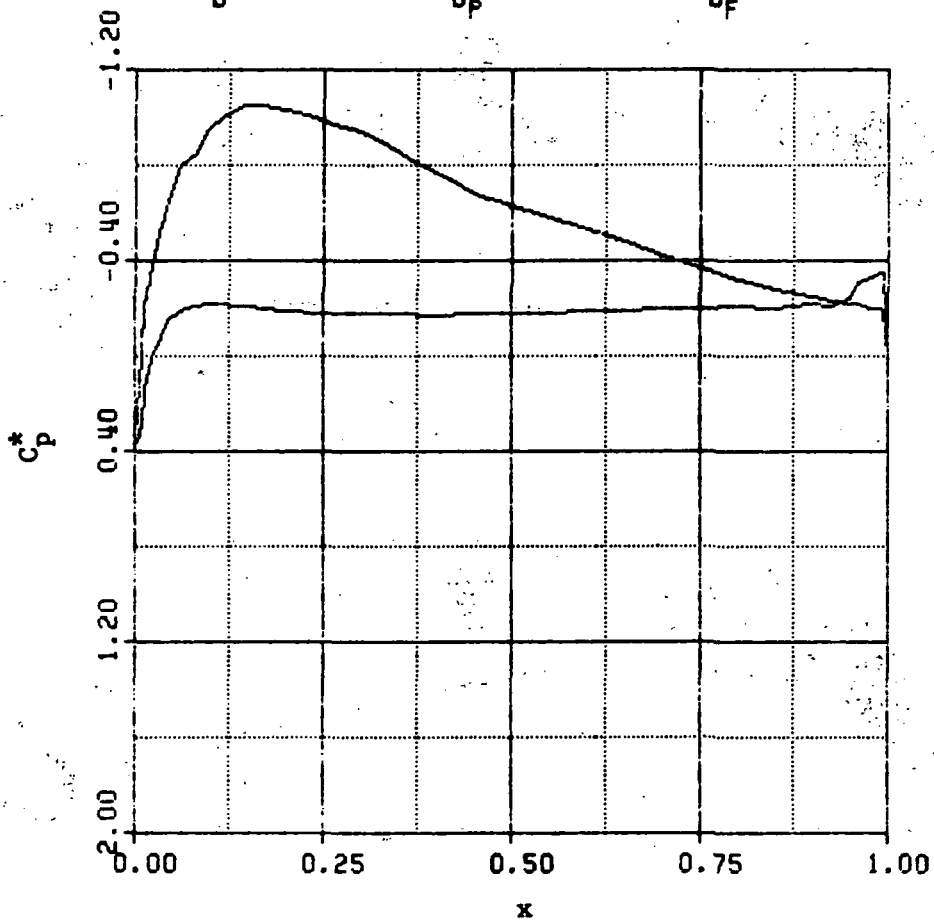
TIME=0.1180

$C_L=0.830511$

$C_D=0.258096$

$C_{Dp}=0.090355$

$C_{Df}=0.167741$



(a) $t = 0.118$.

Figure 17.- Pressure distribution for Göttingen 625 airfoil.

PRESSURE DISTRIBUTION

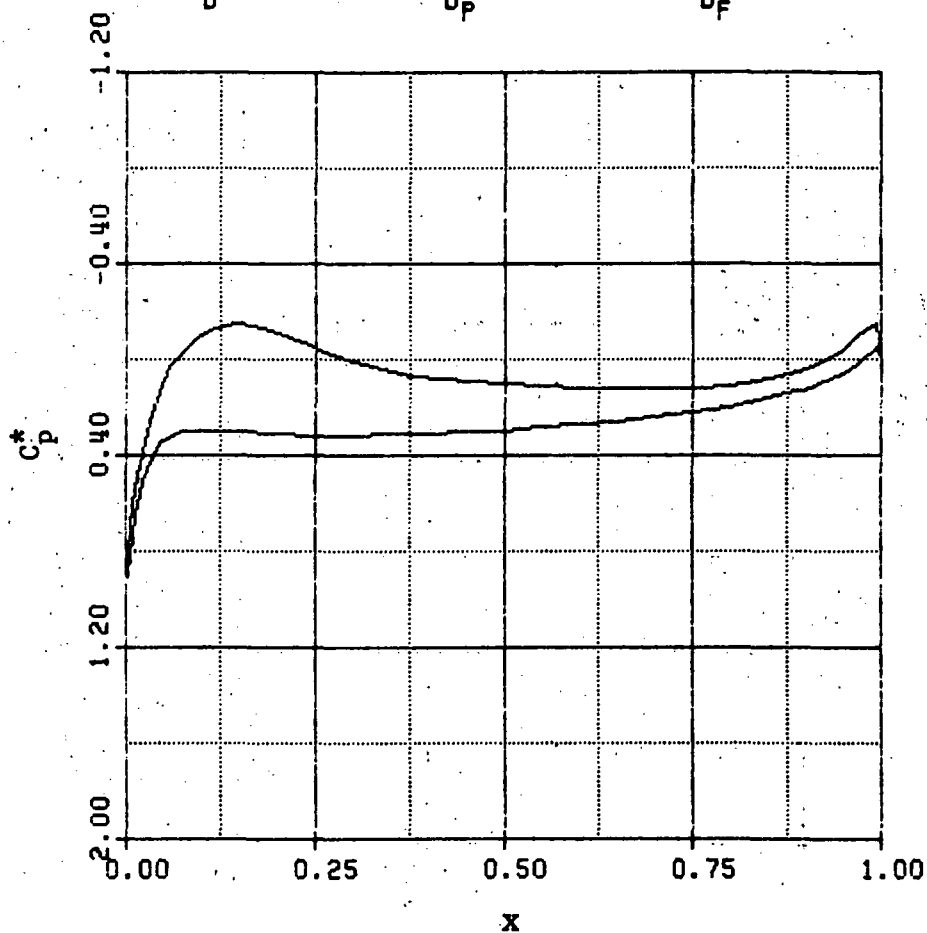
GÖTTINGEN 625 AIRFOIL

ANGLE OF ATTACK=5.00 REYNOLDS NUMBER=2000

TIME=3.3300

$C_L=0.415316$

$C_D=0.229930$ $C_{Dp}=0.153614$ $C_{Df}=0.076316$



(b) $t = 3.33$.

Figure 17.- Concluded.

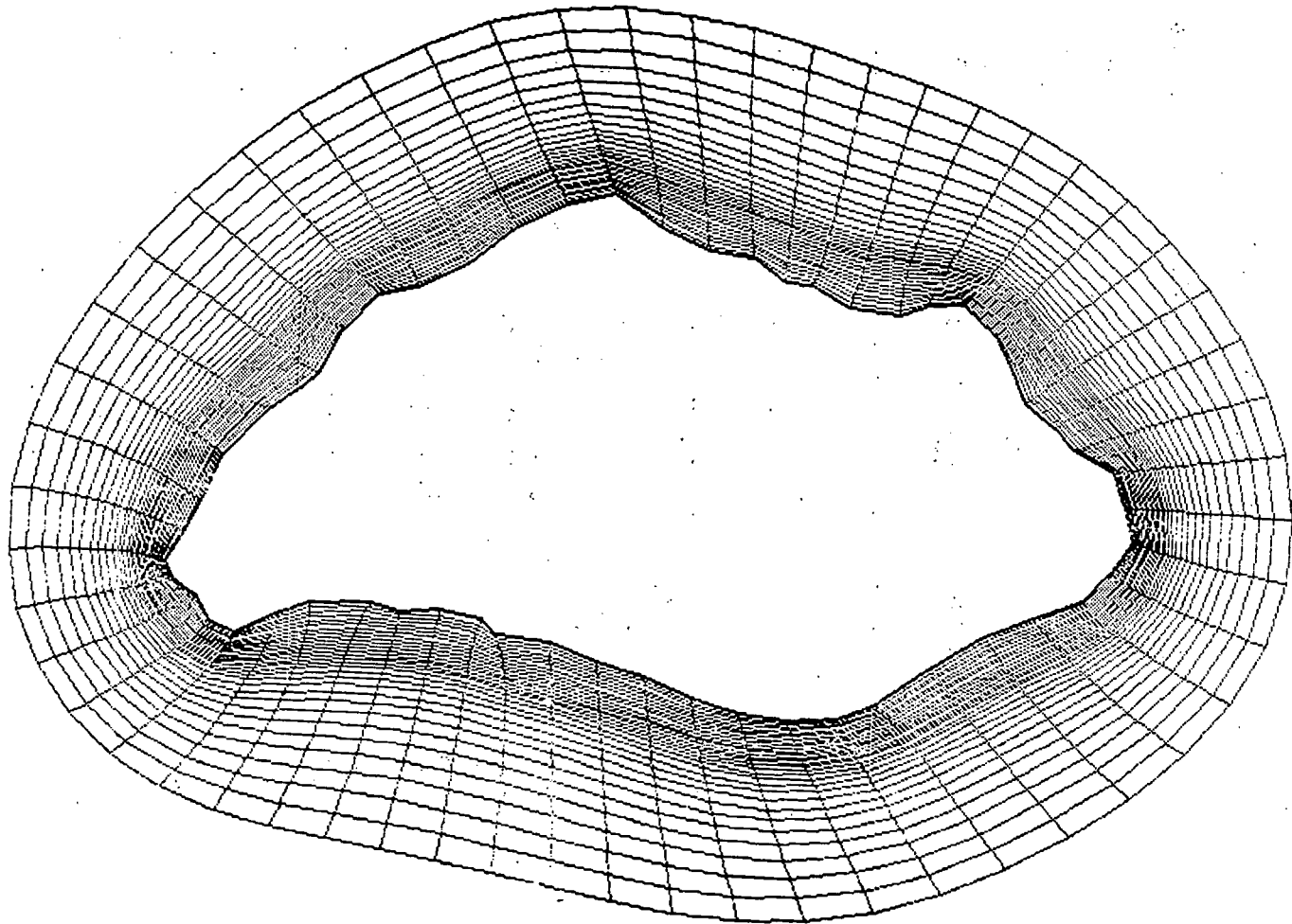
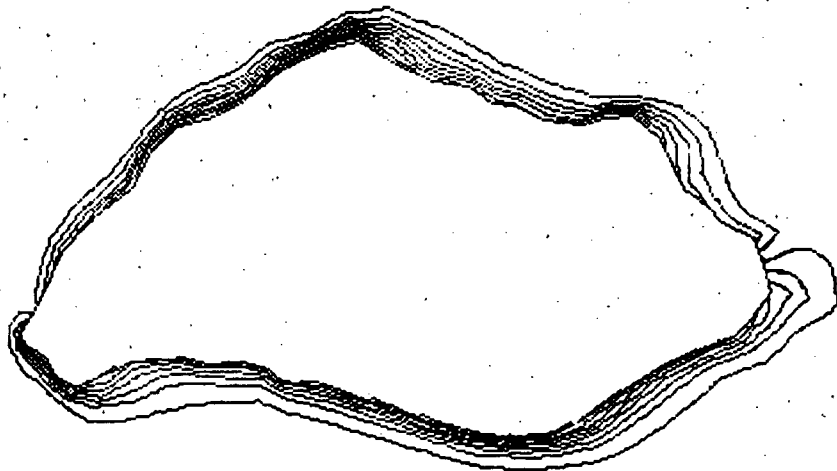
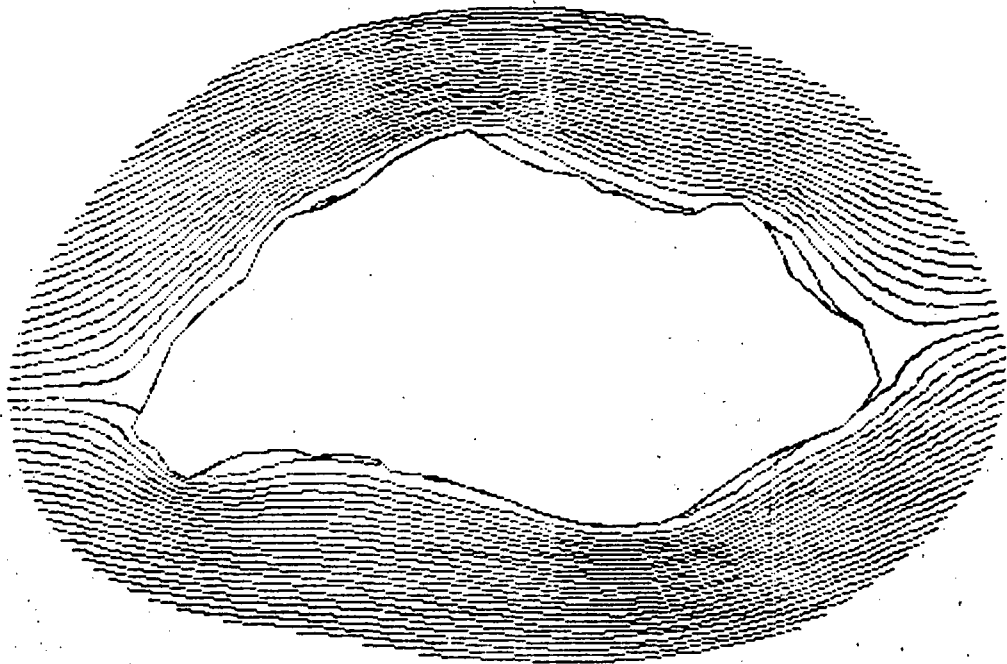
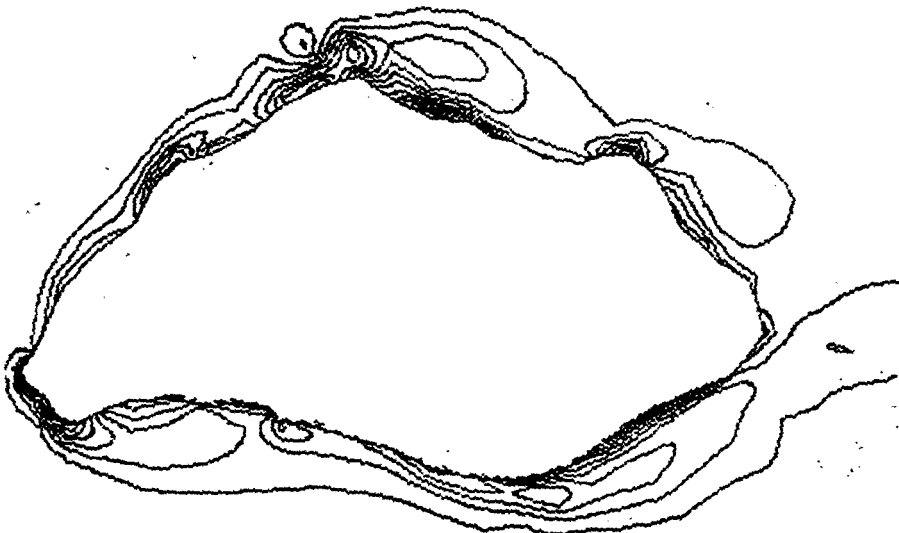
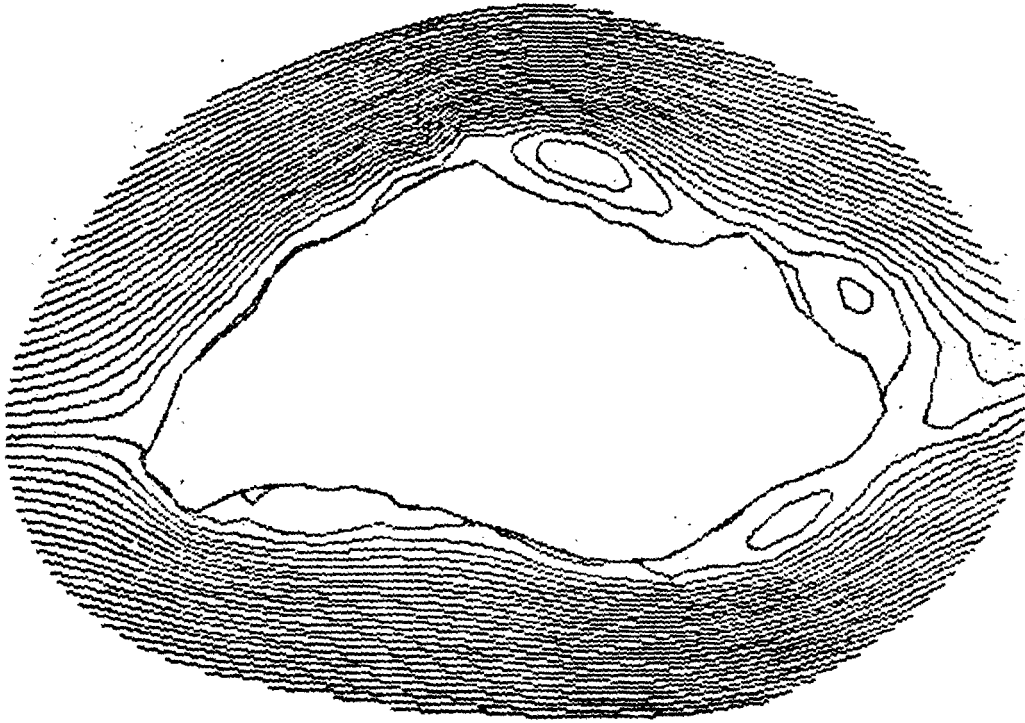


Figure 18.- Contracted coordinate system for cambered rock.

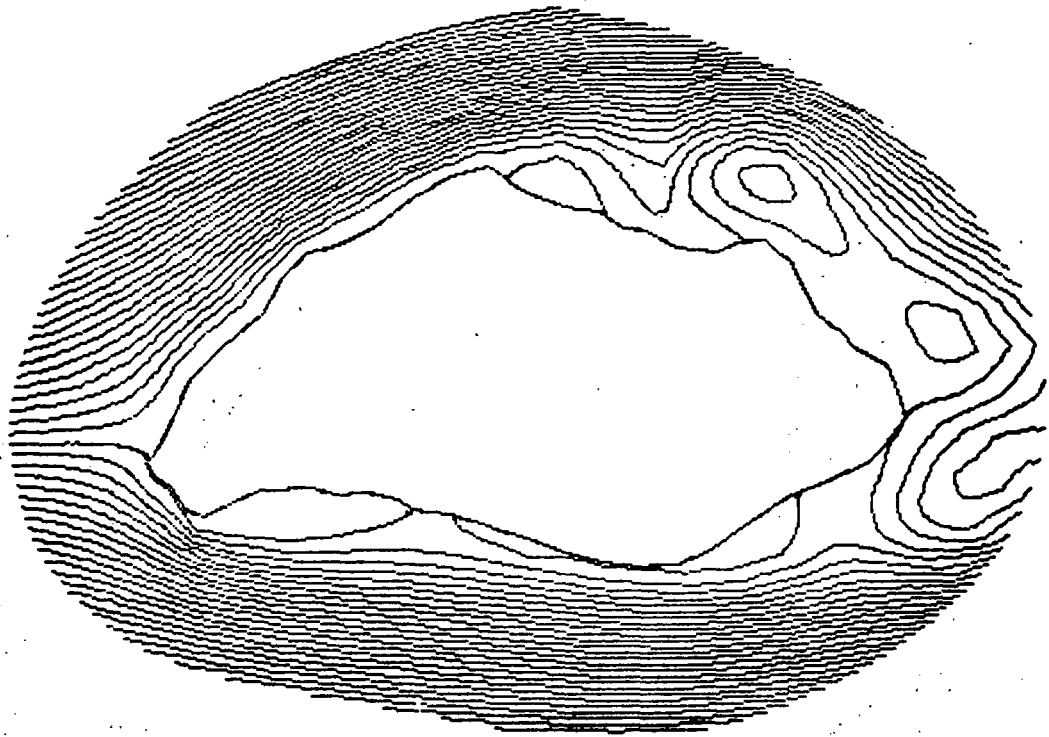


(a) $t = 0.15$.

Figure 19.- Stream-function and vorticity contours for cambered rock.

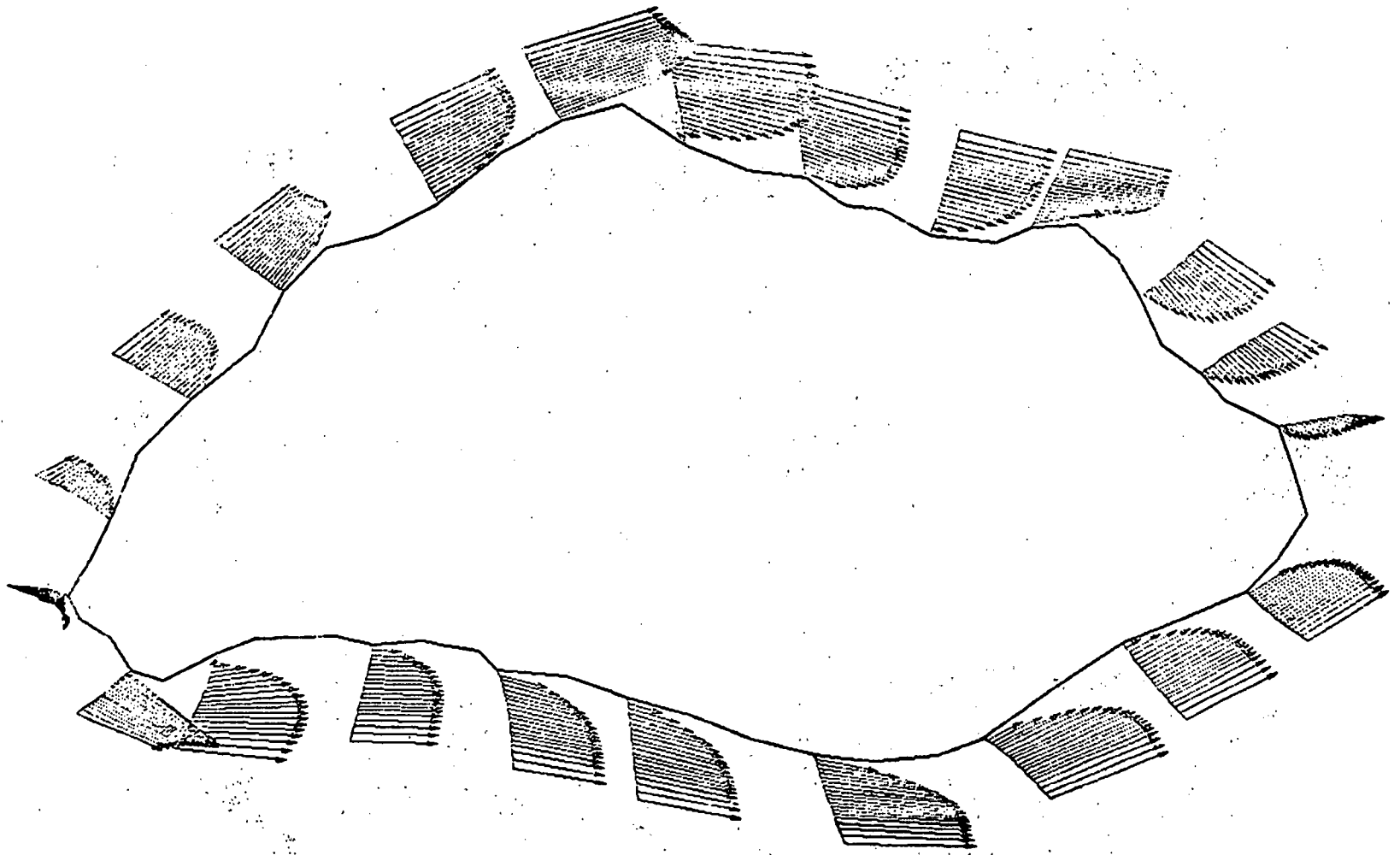


(b) $t = 0.5$.
Figure 19.- Continued.



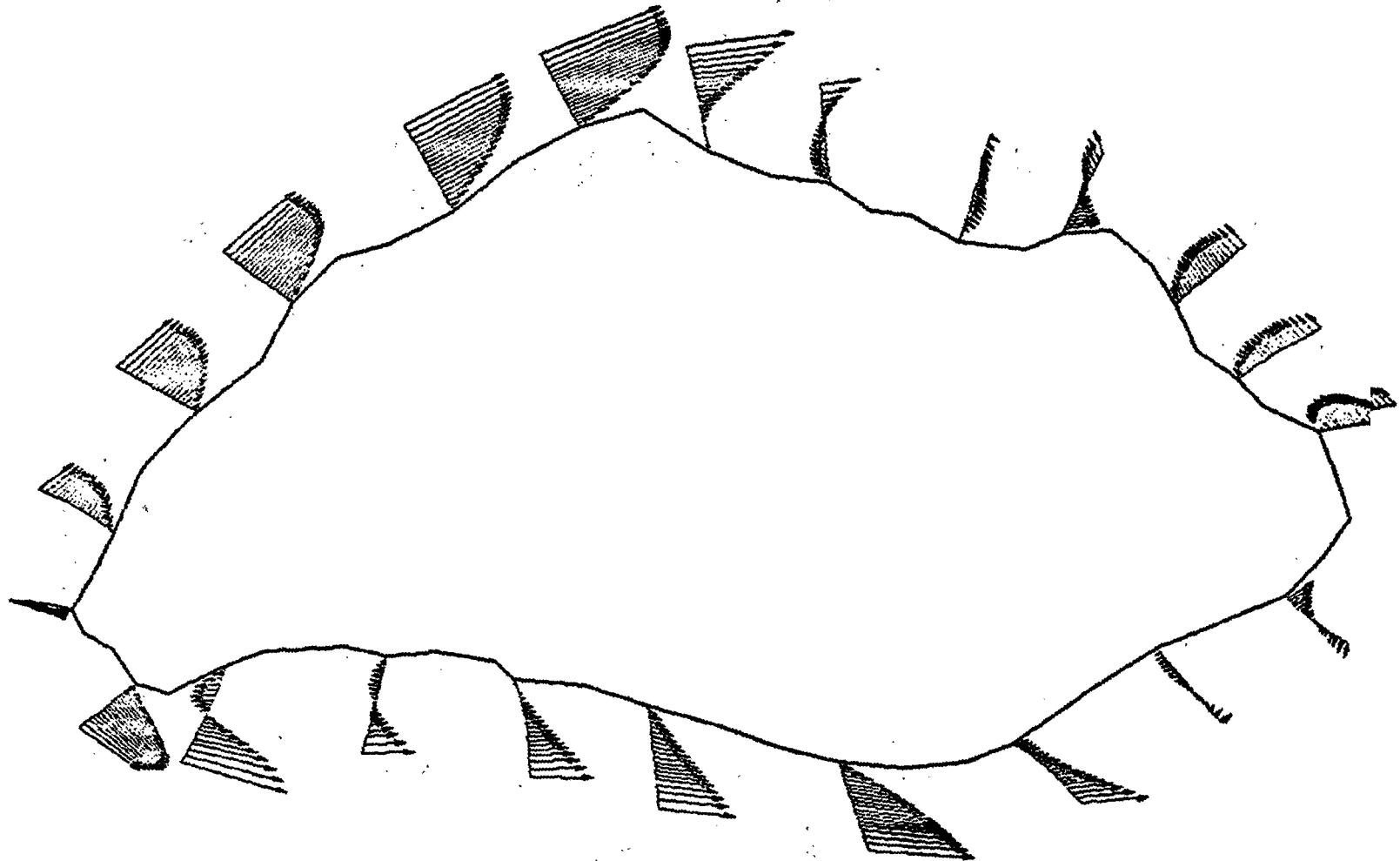
(c) $t = 1.0$.

Figure 19.- Concluded.



(a) $t = 0.1.$

Figure 20.- Velocity profiles for cambered rock.



(b) $\tau = 1.2$.
Figure 20.- Concluded.

PRESSURE DISTRIBUTION

CAMBERED ROCK

ANGLE OF ATTACK=5.00

REYNOLDS NUMBER=500

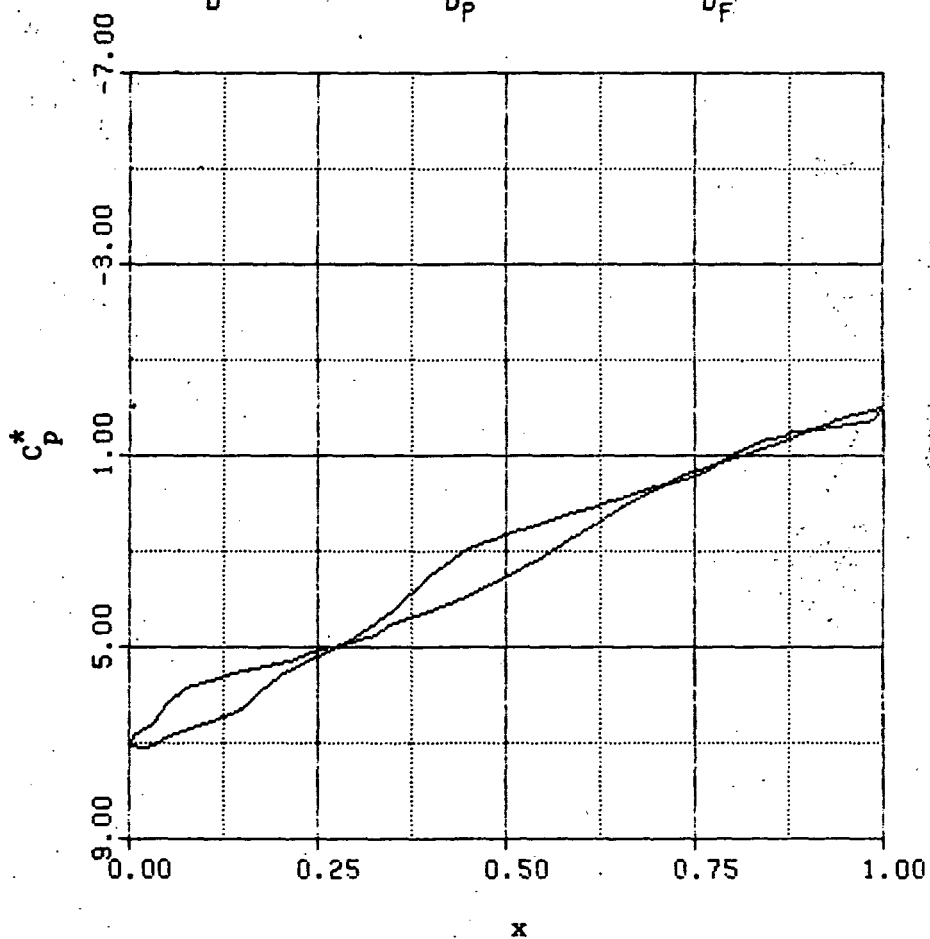
TIME=0.1000

$C_L = -0.281309$

$C_D = 5.439651$

$C_{D_P} = 4.913617$

$C_{D_F} = 0.526034$



(a) $t = 0.1$.

Figure 21.- Pressure distribution for cambered rock.

PRESSURE DISTRIBUTION

CAMBERED ROCK

ANGLE OF ATTACK=5.00

REYNOLDS NUMBER=500

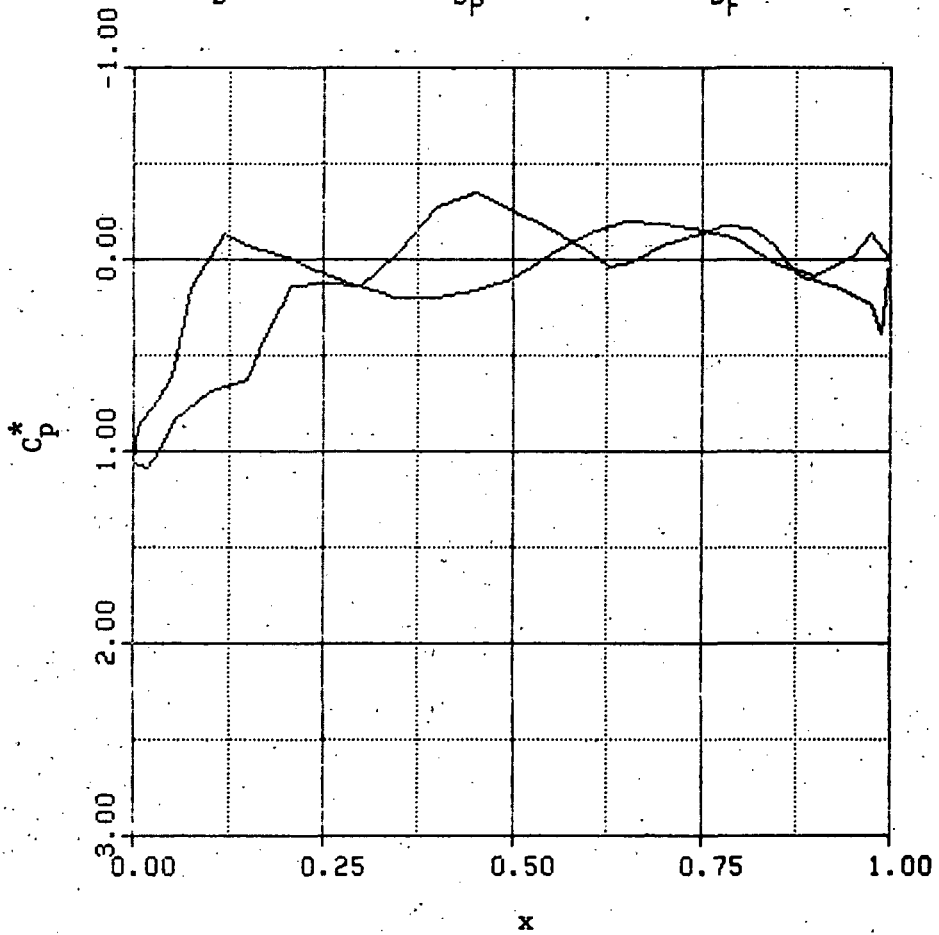
TIME=1.2000

$C_L = -0.118646$

$C_D = 0.624591$

$C_{Dp} = 0.512546$

$C_{Df} = 0.112046$



(b) $t = 1.2$.

Figure 21.- Concluded.